STELLAR EVOLUTION WITHIN AND OFF THE MAIN SEQUENCE[1,2]

By Icko Iben, Jr.

Massachusetts Institute of Technology
Cambridge, Massachusetts

INTRODUCTION

During the past five years, considerable progress has been made in our understanding of stellar evolution during and beyond the hydrogen-burning phases. Through ingenious approximations which reduce the labor of integration and yet retain the basic features of the physical description, Japanese workers have followed stellar evolution from the early stages of pre-main-sequence contraction through and somewhat beyond the shell helium-burning stage. In Germany and the United States several groups have exploited the speed and capacity of available digital computers to construct, by relaxation techniques, nearly uninterrupted sequences of models covering the same range but showing considerably more detail, particularly in the transitional phases between major periods of nuclear burning.

Among Population I stars outside the main-sequence band, the observed regularities for which one can now account in terms of the properties of helium-burning models have become sufficiently numerous that it is almost fair to say that we understand evolution through helium-burning phases for Population I stars nearly as well as we understand evolution through pure hydrogen-burning phases. This does not mean that the description of either the hydrogen- or helium-burning phases is complete. There are still serious gaps and uncertainties in the description of such stars, as well as quantitative inconsistencies between theory and observation.

The effects of mass loss, rotation, and neutrino processes on evolutionary characteristics during the hydrogen- and helium-burning phases have not yet been fully studied. The evolution of close binaries has barely been touched upon. As there is evidence that many "cataclysmic" variables owe their behavior to the presence of a close companion, it is clear that this latter area of research is important.

In this review, attention will be restricted to theoretical studies of stars in the hydrogen- and helium-burning phases and to comparisons between these studies and observation. Emphasis will be placed on work that has not been reviewed by Schwarzschild (1), by the Burbidges (2), by Hayashi, Hōshi & Sugimoto (3), and by Sears & Brownlee (4). An extensive bibliography of recent ($\geq$1958) studies of stellar interiors has been prepared by Langer, Herz

[1] The survey of literature for this review was concluded December 31, 1966.

[2] Supported in part by the National Science Foundation (GP-6387) and in part by the National Aeronautics and Space Administration (NsG-496).

& Cox (5). The large number, 834, of entries in this compilation demonstrates the practical impossibility of doing justice, in a short review, to all work in the field of stellar evolution. The selection of papers for explicit citation has been necessarily somewhat arbitrary and has been centered about the reviewer's own special interests.

THE EVOLUTION OF A $5M_\odot$ POPULATION I STAR

A description of the evolution of a metal-rich star of $5M_\odot$ illustrates recent advances in the study of Population I stars that begin their nuclear-burning life on the upper main sequence. The evolution of models of $5M_\odot$ has been carried further than for models of any other mass (6–8). Moreover, evolution through the core helium-burning phase has been examined by several investigators with varying input physics (8–10); this has offered an opportunity for intercomparison and the assessment of theoretical uncertainties.

The evolutionary track of a $5M_\odot$ model of Population I characteristics is sketched in Figure 1. Numbered circles along the path denote boundaries of easily distinguished phases. Brief descriptions and approximate time scales for each phase are also supplied.

The track in Figure 1 is a rough, order-of-magnitude map which exhibits the basic features of all $5M_\odot$ models constructed to date (8–10) prior to the shell helium-burning phase. The track and time scales between points 1 and 12 are taken from Iben (10). The initial composition is $(X, Y, Z) = (0.71, 0.27, 0.02)$ and $(l/H_d) =$ (mixing length/density scale height) $= 0.5$. The track beyond point 12 is topologically equivalent to that given by Kippenhahn, Thomas & Weigert (8) but is at variance with tracks obtained by Hofmeister (9).

Core Hydrogen Burning

During the main-sequence or core hydrogen-burning phase (points 1–2), hydrogen is converted into helium via the CN-cycle reactions near the center of a large convective core. Mixing causes the hydrogen concentration to drop steadily in a region large compared to the region of significant nuclear-energy production. Throughout the main-sequence phase, the mass fraction in the convective core decreases. For the particular choice of composition that gives the track in Figure 1, the convective-core mass fraction drops steadily from about 0.2 to 0.08 before diminishing rapidly to zero following the phase of overall contraction (near point 3).

If, as has been customary, one assumes that the abundance of N^{14} remains fixed in energy-generating regions, one finds that the central portion of the star contracts and heats throughout the main-sequence phase (8, 9). According to the usual interpretation of this phenomenon, as the average number of particles per gram decreases in the convective core, the balance between pressure forces outward and gravitational forces inward can be maintained only by an increase in density and hence, by virtue of the virial theorem, by

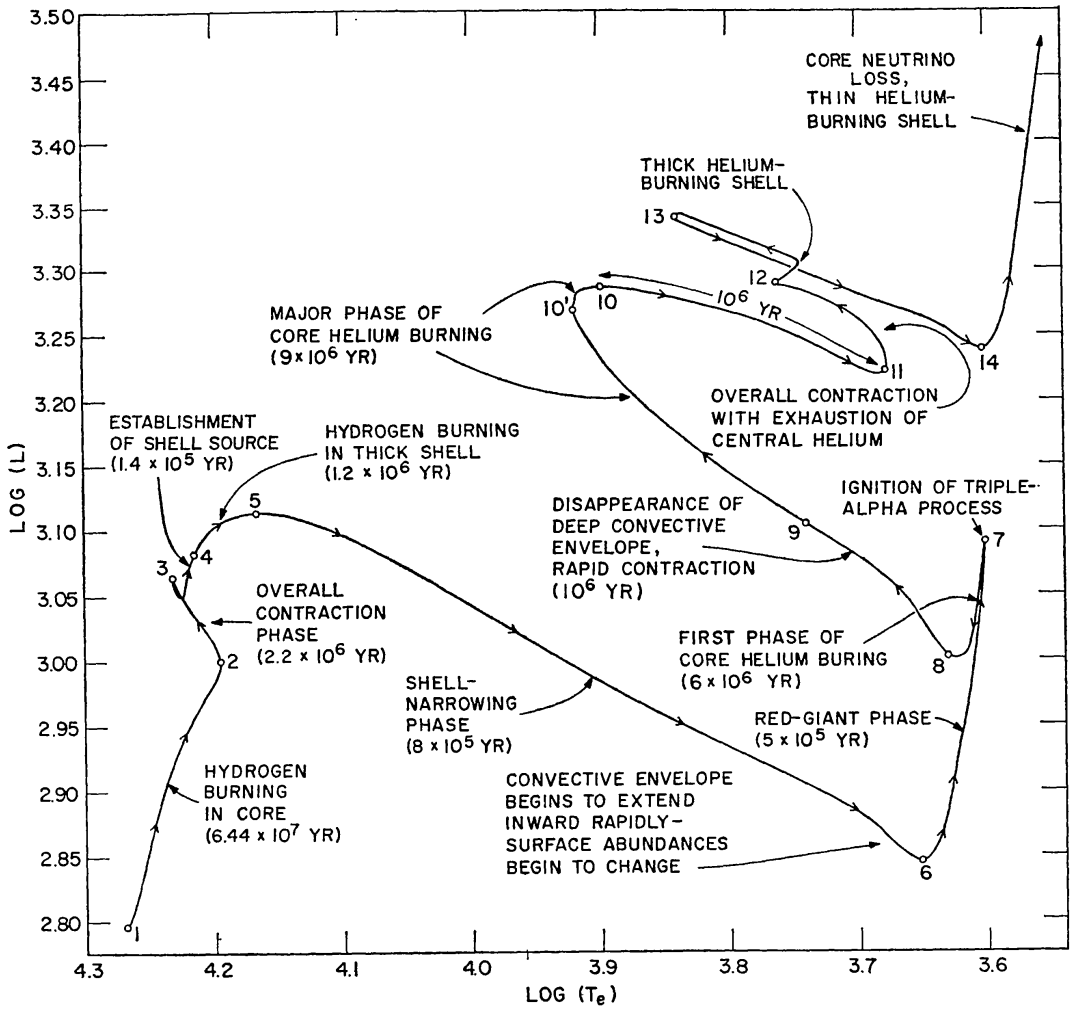

FIG. 1. The path of a metal-rich $5M_\odot$ star in the Hertzsprung-Russell diagram. Luminosity is in solar units, $L_\odot = 3.86 \times 10^{33}$ erg/sec, and surface temperature T_e is in deg K. Traversal times between labeled points are given in years.

heating. Since nuclear sources are highly temperature sensitive, rising core temperatures lead to an increase in stellar luminosity, in agreement with numerical results.

In a real Population I star the abundance of N^{14} does not remain fixed in energy-generating regions. As a result of the reactions $O^{16}(p,\gamma)F^{17}(\beta^+\nu)O^{17}(p,\alpha)N^{14}$, the abundance of N^{14} increases steadily during the main-sequence phase. Central temperatures *drop* during the early portions, and central densities *drop* for a significantly larger fraction, of the main-sequence phase (10). One can argue that in order to maintain a constant energy flux, the increase in the product of the N^{14} and hydrogen abundances must be compensated by a decrease in temperature or density (or both) in energy-generating regions. The increased luminosity during the early period of central cooling and expansion results from the increased concentration of CN-cycle elements.

Once O^{16} has been sufficiently depleted that the product of the H^1 and N^{14} abundances decreases with time, the central regions do contract and heat simultaneously. The rates of heating and condensing accelerate as the core-hydrogen abundance drops until, when the core abundance of hydrogen reaches approximately 0.05 (abundance by mass), the whole star begins to contract. During the ensuing phase of overall contraction (points 2–3), the rate of nuclear-energy production in the convective core remains nearly constant. The increase in luminosity is due primarily to the conversion, in the contracting envelope, of gravitational potential energy into heat and thence into escaping radiation. Toward the end of the phase of overall contraction, the mass fraction in the convective core begins to decrease at an accelerated rate. As the star reaches point 3, the hydrogen abundance in the now rapidly diminishing convective core is reduced to a fraction of 1 per cent.

Shell Hydrogen Burning

Between points 3 and 4, the region of major nuclear-energy production shifts from near the center, where hydrogen becomes exhausted, to a thick shell away from the center, where hydrogen is abundant. The details of this shift are rather complex. Within the central regions, where hydrogen is being exhausted, a finite temperature gradient carries outward a flow of energy which exceeds the rate of nuclear-energy production. The central regions call upon the only other resources immediately available—gravitational potential energy and thermal energy. The hydrogen-impoverished core contracts much more rapidly than during the preceding phase of overall contraction. At the same time, the core also cools; this helps to satisfy the demand for energy. Through cooling more rapidly at the center, the region of hydrogen exhaustion rapidly becomes nearly isothermal. As isothermality is approached, the demand for energy from the core decreases and the rates of core contraction and cooling diminish considerably. At point 4 in Figure 1, the nearly isothermal, hydrogen-exhausted core comprises about 7 per cent of the mass of the star.

While the core is still in the process of contracting and cooling rapidly, hydrogen-rich matter just outside of the region of hydrogen exhaustion is drawn inward to higher densities and temperatures and thereupon ignited. The ignition is mildly explosive, in the sense that matter is pushed away in both directions from the new hydrogen-burning region. Matter throughout the envelope expands outward and the stellar radius increases. Since energy is required to expand matter in the envelope, not all of the nuclear energy generated in the shell reaches the surface. This is the reason for the drop in luminosity immediately following point 3 in Figure 1. It is to be emphasized that between points 3 and 4, the total rate of nuclear-energy production increases with time. Had absorption in the envelope been omitted, as in earlier computations, no drop in luminosity following point 3 would have been detected.

At point 4 in Figure 1, reasonably stable conditions have again been

established. The release of gravitational energy in the hydrogen-exhausted core and the absorption of energy in the stellar envelope are minimal. Between points 4 and 5, nuclear-energy production occurs in a fairly thick shell containing approximately 5 per cent of the star's mass. The shell moves outward (in mass fraction) through the star, adding more mass to the hydrogen-exhausted core, which continues to contract.

The distribution of several composition variables within the $5M_\odot$ star immediately following the phase of overall contraction, between points 3 and 4, is shown in Figure 2 (10). Only the features that are independent of the choice of initial Population I abundances are of interest here.

Wherever hydrogen has been converted almost completely into helium, oxygen has been converted almost completely into N^{14}. Within approximately the inner one half of the star's mass, C^{12} has been converted almost completely into N^{14}. Any initial lithium (not shown) has been destroyed over the inner 98–99 per cent of the star's mass. Similar statements could be made for boron, beryllium, and other light elements. It is worthwhile to point out that considerable quantities of He^3 are made during the main-sequence phase

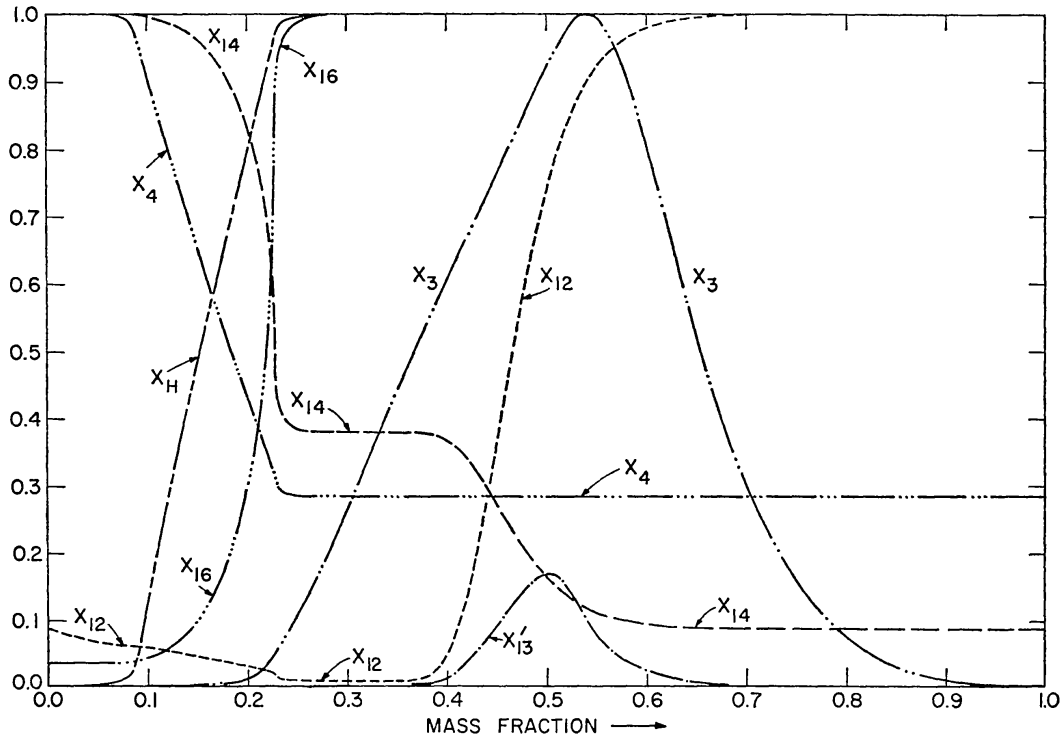

FIG. 2. The variation of composition with mass fraction in the $5M_\odot$ star immediately following the phase of overall contraction (point 3 in Figure 1). The X_i are abundances by mass of $H^1(X_H)$, $He^3(X_3)$, $He^4(X_4)$, $C^{12}(X_{12})$, $C^{13}(X'_{13})$, $N^{14}(X_{14})$, and $O^{16}(X_{16})$. Scale limits correspond to $0.0 \leq X_H < 0.708$, $0.0 \leq X_3 \leq 1.30 \times 10^{-4}$, $0.0 \leq X_4 \leq 0.976$, $0.0 \leq X_{12}$, $X'_{13} \leq 3.61 \times 10^{-3}$, $0.0 \leq X_{14} \leq 1.45 \times 10^{-2}$, and $0.0 \leq X_{16} \leq 1.08 \times 10^{-2}$.

in approximately the middle third of the star's mass, far from regions of significant nuclear-energy production.

As the star approaches point 5 in Figure 1, the mass of the nearly isothermal, hydrogen-exhausted core approaches approximately 10 per cent of the star's mass. A satisfactory physical explanation of why the pressure balance cannot be maintained in an isothermal core when the mass fraction in the core reaches the Schönberg-Chandrasekhar limit (11)—approximately 0.1—has not yet been given. Nor is it understood why core contraction should not proceed rapidly enough to produce a much steeper temperature gradient in the core when the mass fraction is still less than 0.1.

At any rate, as the star evolves beyond point 5, the core begins to contract more rapidly and a sizable temperature gradient is built up as heating occurs preferentially toward the center. Matter in the nuclear-energy-producing shell is drawn more rapidly than before to higher temperatures and densities. Energy production in the shell begins again to be explosive and the stellar envelope expands rapidly. At the same time, the mass of this shell decreases rapidly: e.g. from 3.5 per cent of the star's mass, at point 5, to only 0.5 per cent of the star's mass, at point 6.

Between points 5 and 6, the rates at which temperatures and densities increase within the shell are not sufficient to offset the rate at which the shell narrows and the total rate of nuclear-energy production decreases with time. The decline in the rate of nuclear-energy production is not the only factor contributing to the drop in luminosity. Energy is required to expand the matter in the region between the shell and the surface. Approximately half of this energy is taken from thermal motions in the cooling envelope. The other half is supplied by the shell. In this way the envelope blankets the shell.

Within the expanding and cooling envelope the radiative opacity is increasing. Shortly before point 6, convection becomes the dominant mode of energy transport in a growing region extending inward from the surface.

When the base of the convective envelope reaches the level where lithium has been destroyed during the main-sequence phase, the surface abundance of lithium begins to drop. As the base of the convective envelope sweeps past the corresponding levels for other elements, convective mixing causes the surface abundances of these elements to decrease. Just the reverse, of course, happens to surface abundances of elements that have been formed in the interior during earlier phases, for example He^3 (see Figure 2).

Between the outer edge of the growing convective envelope and the surface, where energy still flows by radiation, the dominant source of opacity is the H^- ion, electrons being supplied by metals of low ionization potential. Instead of increasing with decreasing temperature as in subphotospheric regions, the opacity in the photosphere decreases with decreasing temperature.

Smaller opacities favor a larger energy flow. As the star's surface temperature decreases beyond point 6, its luminosity begins to increase. Within the convective portion of the envelope, the energy required for expansion is supplied entirely by thermal energy. Thus, as the mass of the convective envelope increases, the nuclear source is blanketed less strongly and delivers

a larger fraction of its output to the surface. At the same time, the rate of nuclear-energy production in the shell increases.

As the star's luminosity increases along the red-giant branch, the mass within which nuclear energy is produced continues to decrease. The increased temperatures in the shell more than offset the decrease in shell size.

As the star evolves between points 6 and 7, convection covers more and more of the outer part of the star, reaching almost to the hydrogen-burning shell at point 7. As convection extends into the region where most of the original C^{12} has been converted into N^{14}, mixing begins to carry N^{14} outward and C^{12} inward. As the convective envelope grows, the abundance of N^{14} in the envelope gradually increases while the abundance of C^{12} drops. The ratio of N^{14} to C^{12} in the surface of the star, where it might be observed by the spectroscopist, therefore increases between points 6 and 7. Beyond point 7, the mass of the convective envelope begins to decrease and the surface ratio of N^{14} to C^{12} ceases to change.

During the ascent along the giant branch, central temperatures become sufficiently high that the reactions $N^{14}(\alpha,\gamma)F^{18}(\beta^+\nu)O^{18}$ are ignited. Within a small convective core, N^{14} is rapidly converted completely into O^{18}. Thus, near the stellar center, almost all of the original C^{12}, N^{14}, and O^{16} have been converted into O^{18} by the time the red-giant tip is reached. The only "observable" effect of the $N^{14}\rightarrow O^{18}$ reactions in the stellar core is to prolong the life of the star along the giant branch.

Core Helium Burning

When the star reaches point 7, central temperatures and densities have become high enough that nuclear burning near the center via the triple-alpha process ($3\alpha\rightarrow C^{12}$) alters the course of evolution.

The ignition of the triple-alpha process is explosive in the sense that temperatures and densities near the center at first rise to such values that the rate of nuclear-energy production exceeds the rate at which energy can be transported outward. The energy trapped near the center forces the central regions to expand, causing the temperatures and densities in the hydrogen-burning shell, which still provides most of the star's energy output, to increase less rapidly. Hence, immediately after the triple-alpha ignition at point 7, the luminosity of the star drops.

Between points 7 and 10′, the stellar envelope contracts and the surface temperature increases. This behavior may be ascribed to the fact that the major source of nuclear-energy production is still the hydrogen-burning shell. When averaged over the entire track between points 7 and 10, the shell contributes about 85 per cent of the star's energy output. In order to maintain a balance between energy production and energy outflow, matter in the shell must be kept at sufficiently high densities and temperatures. Since the stellar core continues to expand because of the triple-alpha reactions, this is accomplished through envelope contraction. The contracting envelope tends to heat and compress the hydrogen-rich matter at the leading edge of the shell.

Envelope contraction is particularly rapid between points 8 and 9. This

phase of contraction is not closely connected with nuclear-burning processes in the interior. It is associated with a recession of envelope convection which occurs as a result of decreasing opacity in deep portions of the heating and condensing envelope. As the dominant mode of energy flow switches from convection to radiation, a rapid readjustment of the matter in the envelope ensues. Core helium burning is thus broken into two major phases separated in the H-R diagram by a phase of rapid transit.

The energy flux produced by helium burning leads to the formation of a convective central region. In contrast with its behavior during the main-sequence phase, the convective core *grows* with time during most of the core helium-burning phase (points 7 to 10). At its maximum, the convective core occupies approximately 6 per cent of the star's mass.

As C^{12} increases in the convective core, it reacts with helium to form O^{16}. Whether or not C^{12} reaches an equilibrium abundance depends sensitively on the cross section for the $C^{12}(\alpha,\gamma)O^{16}$ reaction. During the core helium-burning phase, helium also reacts with O^{18} to form Ne^{22}.

Although central densities continue to drop over most of the core helium-burning phase, temperatures in the convective core continue to rise. As the star evolves between points 7 and 8 and between points 9 and 10, the rate of energy production in the core increases relative to the rate of energy production in the hydrogen-burning shell. Except for a brief drop during the phase of rapid envelope contraction (points 8 to 9), the ratio of helium-burning to hydrogen-burning energy-production rates increases steadily from about 0.05 to about 0.36 as the star evolves between points 7 and 10.

As the number of reacting particles in the core decreases, central densities begin to drop less rapidly until, near point 10′, the core begins to contract and the envelope begins to expand. The ensuing phase of core contraction and envelope expansion is reminiscent of the main-sequence phase, when the evolution is controlled by a strong source of energy near the center. The drop in luminosity following point 10 is a result of absorption in the expanding envelope and of a decrease in the strength of the hydrogen-burning shell.

Shell Helium Burning

As the star approaches point 11 and the central helium abundance decreases, the convective core begins to decrease in mass fraction and a larger and larger proportion of the energy produced by helium burning is released outside the convective core. Between points 11 and 12, all parts of the star move toward the center. This phase, associated with the exhaustion of central helium and the formation of a helium-burning shell, is analogous to the phase of overall contraction (points 2 to 3) which precedes the exhaustion of central hydrogen.

Between points 12 and 13, helium burning occurs in a thick shell outside a steadily condensing and heating helium-exhausted core. The strength of the helium-burning shell continues to increase relative to that of the narrow hydrogen-burning shell. As point 13 is approached, and the mass fraction of

the helium-exhausted core reaches approximately 0.07, the helium-burning shell rapidly narrows. The matter between the helium-burning shell and the surface expands outward and cools. The cooling is so great at the hydrogen-helium interface that hydrogen burning temporarily ceases. This occurs shortly beyond point 13 and the hydrogen-helium discontinuity thereafter remains stationary at a mass fraction of about 0.23.

Evolution beyond point 13 is analogous to the earlier phase between points 5 and 7. The core contracts and heats rapidly, while the expanding envelope at first absorbs energy from the narrowing helium-burning shell, whose strength decreases. Over an increasing fraction of the cooling envelope, convective transport dominates over radiative transport. As photospheric opacities drop, the luminosity begins to rise and the star then proceeds again along a "Hayashi" track which is a more luminous extension of the track leading to point 7.

As the star progresses upward along this second giant branch, the base of the growing convective envelope extends deeper into the star, eventually reaching the hydrogen-helium discontinuity marking the position of the inactive hydrogen-burning shell. Mixing then enriches the helium content of the entire convective envelope (6, 8). Convection continues to grow inward until it reaches quite close to the helium-burning shell.

During the ascent along the giant branch following point 14, densities in the helium-exhausted core continue to rise until electrons in the core eventually become relativistically degenerate. When postulated neutrino-loss processes are included, Weigert (7) finds that central regions cool as they contract, most of the energy carried away by neutrinos being supplied from the region of most rapid contraction below the helium-burning shell. The maximum temperature occurs not at the center of the star but in the region of most rapid contraction, and the net rate at which energy escapes in the form of neutrinos is small compared to the rate of nuclear-energy production in the helium-burning shell. The major effect of the neutrino processes is thus to prolong the period of pure shell burning along the giant branch. The refrigerating action of neutrino losses from central regions prevents carbon in the core from burning.

When plasma- and photoneutrino-loss processes are not included, Kippenhahn et al. (8) find that central regions heat as the star ascends the giant branch beyond point 14. Eventually carbon burning is ignited explosively in the relativistically degenerate core. In the ensuing "carbon-flash," energy produced by the conversion of carbon into heavier elements remains in the central regions of the star, heating and expanding these regions until the degeneracy is lifted. Matter near the carbon-helium interface is carried out to such low densities and temperatures that the helium-burning shell becomes inactive. At the same time, the hydrogen-helium interface is heated and a hydrogen-burning shell is reactivated. In a period of 10,000 years the entire process is completed. Thereafter carbon burning continues near the center of a large convective core, in which electrons are no longer degenerate, and a

hydrogen-burning shell moves outward, in mass fraction, forcing the base of the convective envelope to recede ahead of it. The helium-burning shell remains almost inactive.

Schwarzschild & Härm (12) have shown that helium burning in a sufficiently thin shell is thermally unstable. Energy produced in the shell is trapped there, raising the temperature and increasing the rate of energy production until the stored thermal energy is sufficient to expand the overlying material whose mass is large compared to the mass of the shell. The shell then cools and its source strength decreases. Eventually the matter above the shell falls back, compressing the shell until the process begins again.

Weigert (7) has followed the early growth of thermal instability in a $5M_\odot$ star in which the carbon core cools as the star evolves upward along the giant branch. Thermal instability occurs when the mass fraction in the helium-burning shell is roughly 2×10^{-4}. The time interval between successive pulses is roughly 4000 years and the amplitude of each new pulse is larger than that of earlier ones. Whether the amplitude asymptotically approaches a modest final value or whether pulses become sufficiently violent to result in the ejection of mass from the star has yet to be determined.

Uncertainties

How much confidence should one have in the theoretical results just described? There are three questions to be answered.

For a given initial composition, to what extent do uncertainties in the opacity, the convective-flow parameters, and the energy-generation rates affect the general features of the evolutionary track?

How sensitive are evolutionary features to composition changes within the limits of Population I?

Do "perturbations" such as rotation and mass loss alter evolutionary characteristics in an important way?

Answers to all of these questions must at present be partial and somewhat qualitative. A discussion of the third question will be deferred.

On the basis of models thus far published, one may infer that during pure hydrogen-burning phases (points 1–7 in Figure 1), the qualitative relationship between characteristic segments of the evolutionary track is both unaffected by uncertainties in the constitutive relations and invariant to changes in initial composition (within Population I limits). Over this range of evolution, the relationship between changes in observable characteristics and changes in interior processes is common to all nonrotating, constant-mass models of $5M_\odot$.

In contrast, the topology of the evolutionary track during the helium-burning phases, in particular during the phase of helium burning in a thick shell, appears to be highly sensitive to composition changes and is considerably affected by known uncertainties in the constitutive relations. Changes in the initial composition appear to have drastic consequences for the nature of

the evolutionary track and hence for the relationship between this track and the state of the deep interior.

Thus, as evolution progresses to lower surface temperatures and through more advanced nuclear-burning stages, not only does the magnitude of the uncertainties increase, but the *effect* of all the uncertainties is magnified.

Several reasons for this state of affairs are clear. The description of energy flow is particularly incomplete at the low temperatures and densities found in stellar envelopes. The lower the surface temperature and the larger the stellar radius, the larger is the volume of the star affected by incompletely known opacities and unknown parameters in an *ad hoc* treatment of convection. Further, helium-burning reactions have not yet received the attention accorded to hydrogen-burning reactions and are less susceptible to direct experimental study. Finally, the more complex the internal structure of the star, the more precarious is the balance between the various factors and hence the greater is the sensitivity to changes in composition and to uncertainties in the constitutive relationships.

A sample of the variations in main-sequence properties obtained in recent investigations is presented in Table I. Luminosities and surface temperatures are given at the equivalents of points 1 and 2 in Figure 1. The main-sequence lifetime is given by t_{12} and $(M_{cc})_{max}$ represents the maximum mass fraction in the convective core during the main-sequence phase.

Presumably, the only major differences in input physics between cases *b* and *c*, and also between cases *a* and *d*, lie in the choice of opacities, which presumably differ significantly only in the outer layers, where bound-bound contributions to opacity are important. Line contributions to opacity are included in cases *c* and *d*, but not in cases *a* and *b*.

As may be seen from Table I, the actual choices of, or approximations to, interior opacities in cases *b* and *c* are sufficiently different that the maximum convective-core mass is 15 per cent smaller and the initial luminosity is 9 per cent larger in case *c* than in case *b*. These differences can occur only if interior opacities in case *c* are *smaller* than in case *b*, a rather surprising result if one supposes that including additional sources of opacity would lead to higher

TABLE I

VARIATIONS IN MAIN-SEQUENCE PROPERTIES

Investigator	Case	Composition		$\log (L/L_\odot)$		$\log (T_e)$		$(M_{cc})_{max}$	$t_{12}(10^7$ yr)
		X	Z	(1)	(2)	(1)	(2)		
10	*a*	0.708	0.02	2.79	3.00	4.269	4.195	0.225	6.44
8	*b*	0.602	0.044	2.78	3.00	4.245	4.194	0.212	5.37
9	*c*	0.602	0.044	2.82	2.99	4.236	4.173	0.185	4.83
9	*d*	0.739	0.021	2.66	2.87	4.223	4.150	—	8.71

opacities. One might also have expected a more pronounced difference in surface temperature between cases *b* and *c*. It has been shown (13) that, for the initial main-sequence model, the inclusion of line effects reduces log (T_e) by about 0.03. The differences between cases *a* and *d* are in the direction expected, but of sufficient magnitude to suggest that not only uncertainties in opacity but also uncertainties introduced by the *approximations* to opacities used by different investigators can have a surprisingly large effect on main-sequence properties.

Unfortunately, the effect of altering the initial hydrogen abundance or the initial heavy-element abundance separately cannot be deduced from Table I. However, one may note, on comparing cases *c* and *d*, that a variation of composition parameters within Population I limits can significantly alter the main-sequence lifetime.

Variations in observable properties following the main-sequence phase are compared quantitatively in Table II. Logarithms of luminosity and surface temperature are given at points corresponding to the numbering in Figure 1. Times (in units of 10^7 yr) refer to the interval between successive points in Table II. Only selective comments will be made.

The mean value of log T_e along the giant branch, $\langle \log T_e \rangle_{RG}$, differs by $\sim$0.04 among the exhibited cases. Hofmeister (9) has shown that an increase of only 40 per cent in the ratio of mixing length to pressure scale height can increase $\langle \log T_e \rangle_{RG}$ by 0.05. It may be concluded that for a given initial composition, $\langle \log T_e \rangle_{RG}$ is uncertain by at least 0.1.

The giant-branch phase (points 6 to 7) lasts longer in case *a* than in all other cases because only in case *a* have the reactions $N^{14}(\alpha,\gamma)F^{18}(\beta^+\gamma)O^{18}$ been included. At the red-giant tip, in case *a*, convection occurs over the outer 70 per cent of the star's mass. In case *b*, envelope convection covers a maximum of only 50 per cent of the star's mass. The variation in surface abundances due to mixing is thus uncertain.

The lifetime for the core helium-burning phase is 1.67×10^7 yr for case *c* compared to only 1.1×10^7 yr, or a factor of 1.52 smaller, in case *b*. The reason for the difference presumably lies with the choice of interior opacities. In case *b* the convective core *decreases* in mass fraction from $\sim$0.04 to 0.03, giving an average mass fraction of $\sim$0.035. In case *c*, the mass fraction in the core *increases* from $\sim$0.04 to $\sim$0.05. The amount of fuel consumed during the core helium-burning phase is thus 0.05/0.035 $\sim$1.43 times greater in case *c* than in case *b*. In case *a*, the convective core increases to a maximum mass fraction of 0.06. Since no data concerning the convective core are available for case *d*, no comparison can be made.

Another feature of considerable importance is the maximum blueward extension of the evolutionary track during the core helium-burning phase. From entries in Table II corresponding to point 10′ in Figure 1, it appears that this extension is tremendously sensitive not only to variations in both convective-flow parameters and opacities, but also to variations in the choice of Population I composition. In fact, in case *d* the entire evolutionary track

1967ARA&A...5..571I

TABLE II

VARIATIONS IN OBSERVABLE CHARACTERISTICS

Point	(a)			(b)			(c)			(d)			Description ($i \rightarrow j$)
	log L	log T_e	t_{ij}	log L	log T_e	t_{ij}	log L	log T_e	t_{ij}	log L	log T_e	t_{ij}	
1	2.80	4.27		2.78	4.24		2.82	4.24		2.66	4.22		
2	3.00	4.20	6.44	3.00	4.19	5.37	2.99	4.17	4.83	2.87	4.15	8.71	Main sequence
3	3.06	4.23	0.22	3.08	4.24	0.25	3.08	4.22	0.23	2.93	4.19	0.25	Overall contraction
5	3.11	4.17	0.14	3.16	4.14	0.20	3.12	4.15	0.08	2.97	4.12	0.19	Hydrogen burning in thick shell
6	2.84	3.65	0.08	2.85	3.68	0.08	2.59	3.68	0.09	2.47	3.67	0.13	Shell narrowing
7	3.09	3.60	0.049	3.00	3.64	0.025	2.87	3.64	0.023	2.90	3.63	0.033	Red-giant branch
10	3.27	3.92	1.44	3.13	3.79	0.81	3.01	3.75	1.29	2.77	3.65	1.78	Core helium burning
11	3.22	3.68	0.19	3.10	3.66	0.29	2.99	3.64	0.38	2.96	3.63	0.42	
13	estimate		0.2–0.3	3.29	3.77	0.79	2.95	3.66	0.07	2.85	3.64	0.07	Helium burning in thick shell
>14	—	—	—	Giant branch		0.03	Giant branch		0.41	Giant branch		0.80	

during helium burning is confined to the giant branch. The major cause for the difference between cases *c* and *d* must be the difference in envelope hydrogen content, since decreasing Z for fixed initial X has the opposite effect from that obtained.

The maximum extention to the blue is also influenced by the relative rates at which C^{12} is created and destroyed. If the cross-section factor for the reaction $C^{12}(\alpha,\gamma)O^{16}$ is reduced from the theoretical maximum to one-tenth of the maximum, log T_e at point 10′ in Figure 1 is decreased by $\sim$0.06 (10). Note that the center-of-mass cross-section factor for the reaction $C^{12}(\alpha,\gamma)O^{16}$ in case *c* is chosen to be about one tenth of the theoretical maximum, whereas $C^{12}\rightarrow O^{16}$ conversion is neglected entirely in case *b*. Yet log T_e at point 10′ is *smaller* in case *c* than in case *b* by $\sim$0.04. This suggests that the inclusion of line absorption in the opacity can decrease the maximum extension to the blue during core helium burning by at least 0.1 in log T_e, unless of course the evolutionary track is already compressed to the giant branch.

The uncertainty in the magnitude of the reaction $C^{12}(\alpha,\gamma)O^{16}$ also introduces an uncertainty as to the end products of helium burning. If the maximum cross-section factor is chosen, the end product is entirely O^{16}. If the cross section is chosen ten times smaller, roughly equal amounts of C^{12} and O^{16} result as end products (9, 10).

Whether the evolutionary track extends to the blue during the phase of helium burning in a thick shell (following point 12 in Figure 1) or whether it proceeds directly to the giant branch appears also to be considerably affected by variations in opacity and in composition choices. The time spent in this phase clearly depends (among other things) on whether the convective core increases or decreases during the preceding core helium-burning phase. In case *b* the maximum blueward extension during the thick-shell phase exceeds the maximum blueward extension during the core helium-burning phase. In case *c* (same initial composition as in case *b*) the thick-shell phase is confined to the giant branch. In case *d* both major phases of helium burning are confined to the giant branch.

VARIATIONS WITH MASS

Evolutionary tracks for several metal-rich stars of different mass are shown in Figure 3. The initial composition and the input physics for all stars represented are the same as for the $5M_\odot$ star described in Figure 1. Solid portions of the tracks in Figure 3 are direct results of computation (10, 14–17); dashed portions are estimates. The times spent by each star in traversing intervals between successive labeled points are given in Tables III and IV.

Model tracks for stellar masses $M \geq 3M_\odot$ are terminated just before the phase of helium burning in a thick shell. Tracks for less massive stars are terminated just before the ignition of helium in the core. For stars of mass $M \leq 1.5M_\odot$, these termination points are estimates.

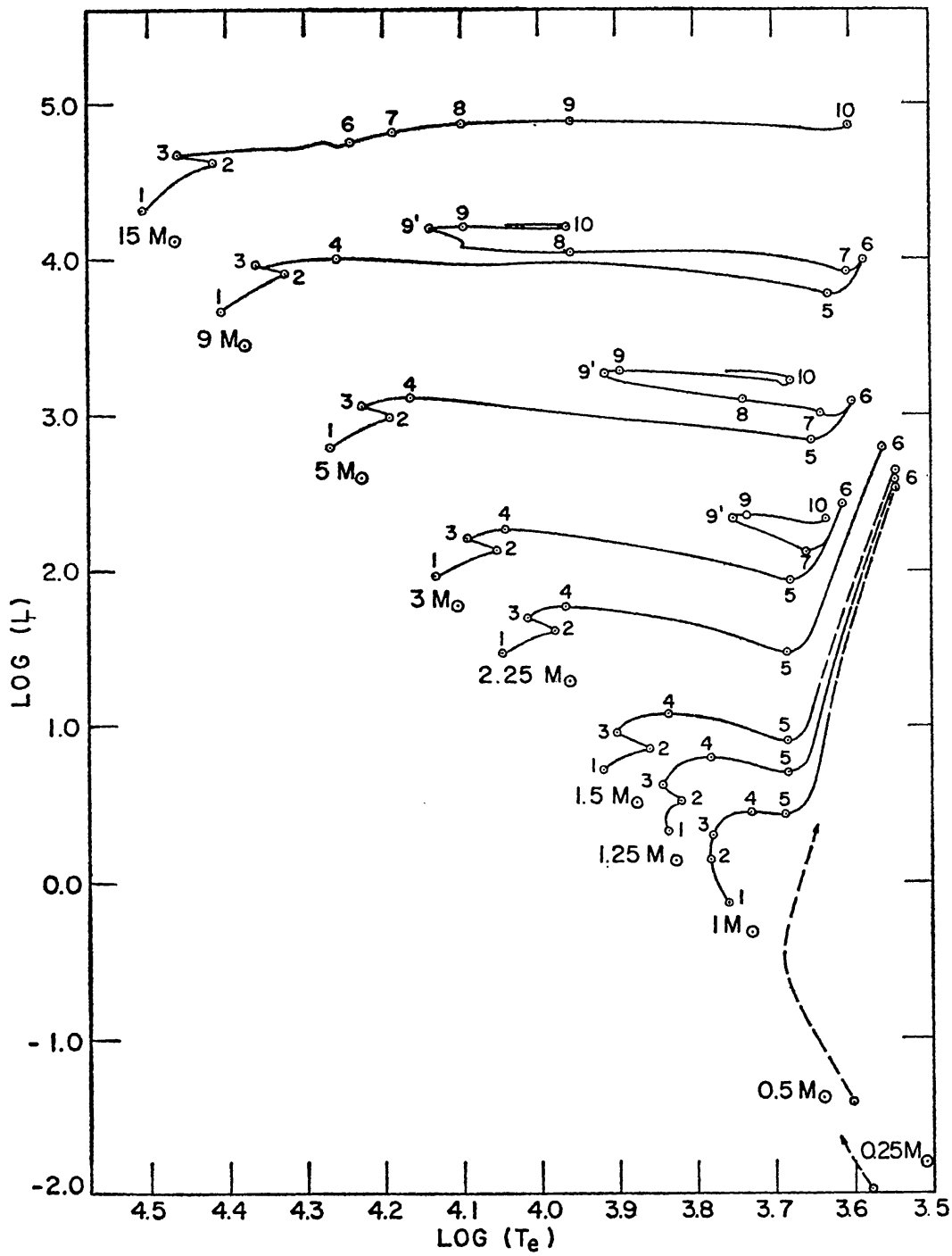

FIG. 3. Paths in the H-R diagram for metal-rich stars of mass $(M/M_{\odot}) = 15$, 9, 5, 3, 2.25, 1.5, 1.25, 1, 0.5, 0.25. Units of luminosity and surface temperature are the same as in Figure 1. Traversal times between labeled points are given in Tables III and IV. Dashed portions of evolutionary paths are estimates.

TABLE III

STELLAR LIFETIMES (yr)[a]

Mass ($M_\odot$) \ Interval (i–j)	(1–2)	(2–3)	(3–4)	(4–5)	(5–6)
15	1.010 (7)	2.270 (5)		7.55 (4)	
9	2.144 (7)	6.053 (5)	9.113 (4)	1.477 (5)	6.552 (4)
5	6.547 (7)	2.173 (6)	1.372 (6)	7.532 (5)	4.857 (5)
3	2.212 (8)	1.042 (7)	1.033 (7)	4.505 (6)	4.238 (6)
2.25	4.802 (8)	1.647 (7)	3.696 (7)	1.310 (7)	3.829 (7)
1.5	1.553 (9)	8.10 (7)	3.490 (8)	1.049 (8)	$\geq$2 (8)
1.25	2.803 (9)	1.824 (8)	1.045 (9)	1.463 (8)	$\geq$4 (8)
1.0	7 (9)	2 (9)	1.20 (9)	1.57 (8)	$\geq$1 (9)

[a] Numbers in parentheses beside each entry give the power of ten to which that entry is to be raised.

TABLE IV

STELLAR LIFETIMES (yr)[a]

Mass ($M_\odot$) \ Interval (i–j)	(6–7)	(7–8)	(8–9)	(9–10)
15	7.17 (5)	6.20 (5)	1.9 (5)	3.5 (4)
9	4.90 (5)	9.50 (4)	3.28 (6)	1.55 (5)
5	6.05 (6)	1.02 (6)	9.00 (6)	9.30 (5)
3	2.51 (7)	4.08 (7)		6.00 (6)

[a] Numbers in parentheses beside each entry give the power of ten to which that entry is to be raised.

THE ZERO-AGE MAIN SEQUENCE

In a first approximation, the variation with mass of stellar properties averaged over the main-sequence phase is roughly the same as the variation of properties of homogeneous models along the zero-age main sequence (points 1 in Figure 3). A summary of the calculated variation with mass of several interior characteristics is given in Figure 4. The lower curve joins model stars on the zero-age main sequence in the mass-luminosity plane. The first three numbers in parentheses beside each mass give, respectively, central density (g/cm^3), central temperature (10^6°K), and stellar radius ($R_\odot$) corresponding to the initial main-sequence position. The fourth number gives the maximum mass fraction in the convective core during the main-sequence phase and the fifth number measures the lifetime of the model star in the main-sequence band.

In none of the initial low-mass models described in Figures 3 and 4 is electron degeneracy of overwhelming importance. At the center of the $1M_\odot$, $0.5M_\odot$, and $0.25M_\odot$ models, electron degeneracy is responsible for 1.7, 2.4, and 6.5 per cent of the total pressure. In the more massive homogeneous stars described in Figure 4, radiation pressure is not negligible. At the center of the $5M_\odot$, $9M_\odot$, and $15M_\odot$ stars, radiation pressure contributes 2.1, 5.1, and 11 per cent of the total pressure.

For stellar masses greater than $\sim 7M_\odot$, the calculated mass-luminosity relationship takes the form $L \propto M^3$. For very light stars, which are completely convective ($M \lesssim 0.4M_\odot$), $L \propto M^{1.68}$. In the neighborhood of $1M_\odot$, $L \propto M^{4.75}$.

The qualitative nature of trends along the zero-age main sequence can be established without reference to detailed computations. The assumption of hydrostatic equilibrium is sufficient to establish that, for the range in mass shown in Figure 4, $\rho_c/T_c^3 \propto \mu^{-3}M^{-2}$, where ρ_c and T_c are central density and temperature and μ is the mean molecular weight. If one further assumes that energy is transferred over most of the interior by radiative diffusion, it follows that $L \propto (\mu^4 M^3/\kappa)$, where κ is a measure of the mean interior opacity. Finally, with a rough knowledge of the magnitude and of the density and temperature dependence of opacity sources and of energy-generation rates, one can establish, still without recourse to detailed computations, that $L \propto M^3$ for stars sufficiently massive that electron scattering is the main source of opacity, whereas $L \propto M^5$ for stars sufficiently small that the p-p chains dominate over the CN-cycle reactions and free-free and bound-free absorption contribute predominantly to opacity.

The variation with mass of the initial central density is interesting. For masses above about $1.25M_\odot$ and below about $0.5M_\odot$, the central density decreases with increasing mass. In the intermediate region, the density increases with increasing mass. The calculated dependence of the central density on mass is consistent with a simple order-of-magnitude argument. Assuming that $\rho_c \propto T_c^3/M^2$ and that $L \propto \rho_c T_c^n M \propto M^{m+1}$, one obtains $(1+3/n)\log \rho_c = \text{const} - (2-3m/n) \log M$. In the high-mass range, where $n \sim 18$ and $m \sim 2$, ρ_c increases as M decreases. In the intermediate-mass range, where $n \sim 4$ and $m \sim 4$, ρ_c decreases as M decreases. In the low-mass range, where $n \sim 5$ and $m \sim 0.7$, density again increases as mass decreases. The values of m required for these statements are obtained, for the high- and intermediate-mass ranges, without detailed calculations. However, for the low-mass stars, which are completely convective except for the region near the photosphere, the mass-luminosity relationship can be obtained only by calculation.

Models along the initial main sequence may be classified, according to the relative importance of the CN cycle and the p-p chains, as belonging to the upper or the lower main sequence. For the composition and physical assumptions here considered, the two sources of energy contribute equally at about $1.9M_\odot$ ($\log L \sim 1.18$).

All upper main-sequence stars have a convective core. With decreasing stellar mass, the mass fraction in the convective core decreases as energy

sources become less strongly concentrated toward the center and as radiation pressure becomes less important. Energy production occurs in a region small compared to the size of the core.

The size of the convective core is not a reliable indicator of the relative importance of the CN cycle. A sizable convective core may occur even along the lower main sequence, where the p-p chains provide more energy than the CN-cycle reactions. For example, in the initial $1.5M_\odot$ model, convection extends over the inner 6 per cent of the star. Three quarters of the total energy output is produced in the core, but less than a quarter of this is contributed by CN-cycle reactions.

The mass at which central convection vanishes is sensitive to the temperature and density dependence of both the opacity and the energy-generation rates. Since interior opacity sources are quite complex for models in the vicinity of $1M_\odot$, one should not rely on the results of a single calculation. For the particular physical assumptions and composition leading to the initial models in Figures 3 and 4, a convective core does not occur for masses and luminosities in the ranges $0.4 < M/M_\odot \leq 1.1$, $-1.6 \leq \log (L/L_\odot) \leq 0.1$.

Models along the lower main sequence with surface temperatures below 8000°K ($\log T_e \leq 3.9$) have relatively extended convective envelopes. The depth of and the mass fraction in the convective envelope increase as stellar mass is lowered until the entire star becomes convective ($M \lesssim 0.4M_\odot$, $\log L \lesssim -1.6$). The uncertainties in surface temperature associated with an inadequate treatment of envelope convection reach a maximum near the center of the ranges $3.6 < \log T_e < 3.9$, $-1, < \log L < +1$. In the neighborhood of $1M_\odot$, a decrease by a factor of 2 in the ratio of mixing length to density scale height lowers the surface temperature by $\Delta(\log T_e) \sim -0.03$ (13). However, the position of stars in the mass-luminosity diagram is not sensitive to changes in the treatment of envelope convection.

Uncertainties in the surface temperature of upper main-sequence models are similar in magnitude to those already described for the $5M_\odot$ model. They are expected to result primarily from uncertainties in envelope opacity. The

---

FIG. 4. Positions in the mass-luminosity diagram, during the main-sequence phase, for the metal-rich stars described in Figure 3. Luminosity and mass are in solar units. The lower curve defines the locus of homogeneous, initial main-sequence models. The first three numbers in parentheses beside each point give central density (g/cm^3), temperature (10^6 °K), and stellar radius ($R_\odot$) for the appropriate model. The upper solid curve represents the locus of models which have just terminated the main-sequence phase, as defined in the text. The dashed curve represents an estimated locus for low-mass models which have evolved for 10^{10} yr. The last two entries in parentheses beside each point give the maximum mass fraction in the convective core and the main-sequence lifetime in years.

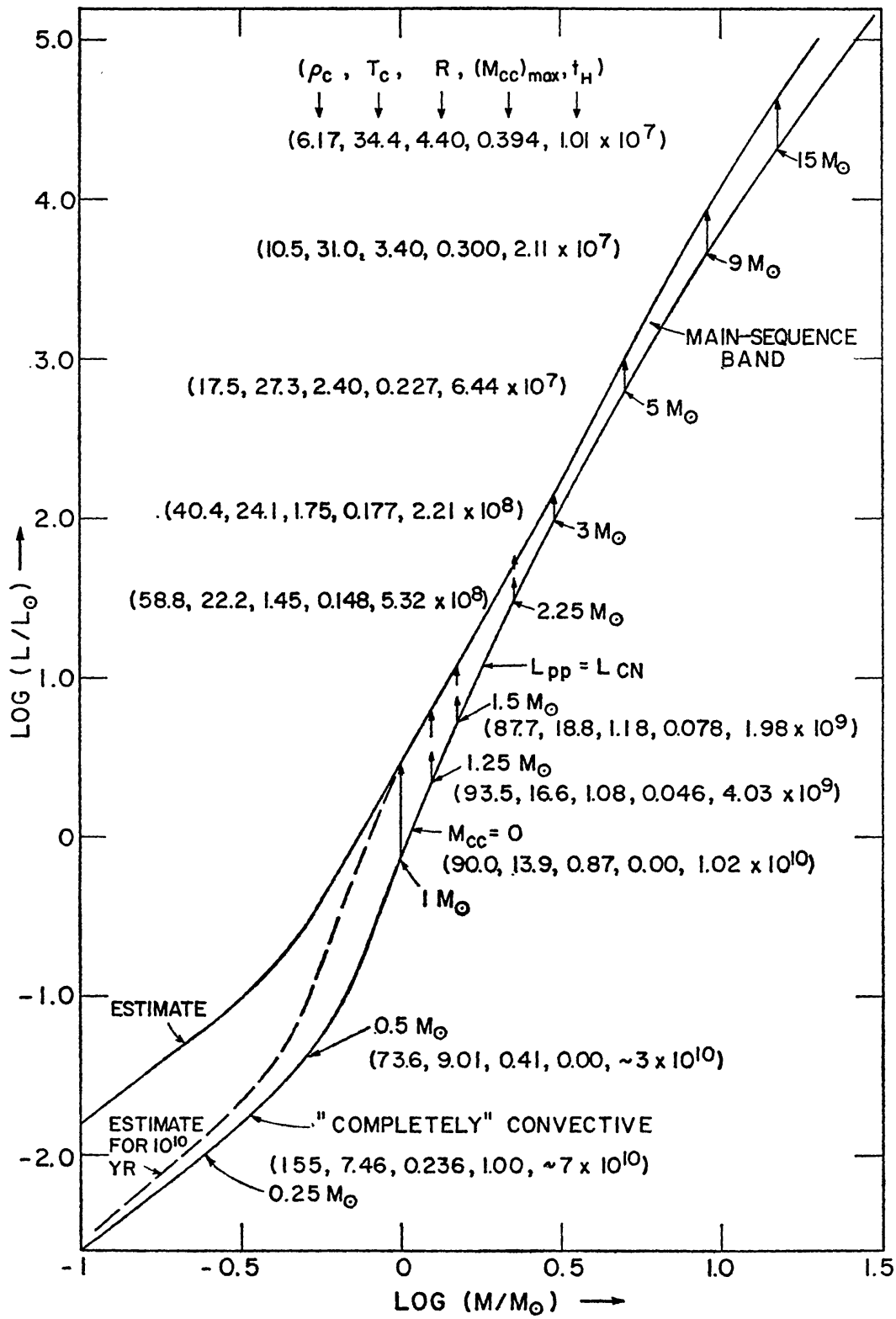

slope of the zero-age main sequence line is expected to be independent of these uncertainties. In particular, the inclusion of line contributions to the opacity lowers the surface temperature uniformly by $\Delta(\log T_e) \sim -0.03$ along the upper zero-age main sequence (13).

A brief summary of the effects of composition changes on the position of the zero-age main sequence is in order. A change in X influences luminosity and surface temperature primarily through the molecular weight. As one reduces the number of particles per gram throughout the star, the necessity of maintaining the pressure balance demands that much of the star contract. The virial theorem implies an increase in interior temperatures which in turn, owing to the temperature sensitivity of nuclear sources, implies an increase in luminosity. A change in Z affects L and T_e primarily through bound-free contributions to opacity.

For a fixed mass, increasing X or Z (or both) lowers model luminosity and surface temperature. For example (13), in the neighborhood of $\log (M) \sim 0.1$, $\Delta(\log L) \sim -(2.5\Delta X + 13\Delta Z)$, whereas near $\log (M) \sim 0.6$, $\Delta(\log L) \sim -(1.9\Delta X + 7\Delta Z)$.

In describing the effect of composition changes on the position of the zero-age main sequence in the H-R diagram, it is best not to focus on individual values of the mass. Over restricted portions of the H-R diagram, the slope of the zero-age line is unaffected by composition changes. One may therefore think of composition changes as shifting the zero-age line bodily either in the vertical direction ($T_e = \text{const}$) or in the horizontal direction ($L = \text{const}$). Along the lower main sequence, in the neighborhood of $\log L \sim 0.0$, the magnitude of the shift obeys the rough relationships (13): $\Delta(\log L) \sim \Delta X + 5\Delta Z$ when $T_e = \text{const}$; and $\Delta(\log T_e) \sim -(0.15\Delta X + 0.8\Delta Z)$ when $L = \text{const}$. In the vicinity of $\log L \sim 2.0$, one has: $\Delta(\log L) \sim 0.66\Delta X + 10.5\Delta Z$ when $T_e = \text{const}$; and $\Delta(\log T_e) \sim -(0.12\Delta X + 1.9\Delta Z)$ when $L = \text{const}$. A measure of the effect of uncertainties in opacities may be obtained by simply altering Z in these expressions by, say, 0.015.

The mass and luminosity level at which the convective core disappears is sensitive to composition (18). From more detailed investigations (19), it is found that the luminosity at which convection disappears varies with composition roughly like $\Delta(\log L) \sim 1.4\Delta X - 4.5\Delta Z$ and that the mass at which central convection disappears varies according to $\Delta(\log M) \sim .9\Delta X + 1.9\Delta Z$.

The Main-Sequence Phase

The fact that relatively massive stars grow redder as they brighten while light stars initially grow bluer is related to the fact that significant helium production occurs over a much larger fraction of the lighter stars. The tendency toward contraction is most pronounced in regions where the molecular weight is increasing most rapidly. Hence, the more evenly molecular-weight changes are spread over the star, the greater is the fraction of the star that contracts and the smaller is the rate of increase of radius relative to the rate of luminosity increase.

For all the stars in Figure 3, the radius increases throughout the phase of core hydrogen burning. In the limit of extremely light stars which are completely convective, the molecular weight increases at the same rate throughout the star. The evolutionary track for such stars may be obtained simply by joining points of constant mass along zero-age main sequences characterized by successively higher values of molecular weight.

The slope of an evolutionary path, $\left| d \log L / d \log T_e \right|$, increases with mass along that portion of the upper main sequence shown in Figure 3. This tendency for the slope to increase with mass is reduced as radiation pressure becomes appreciable. In the limit of high masses, where radiation pressure dominates gas pressure, $L \propto M/(1+X_e)$, where X_e is the abundance of hydrogen in the envelope. Hence the luminosity tends to remain constant whatever the changes in internal composition. The tendency for the evolutionary track to become increasingly horizontal as the mass increases is demonstrated by a series of evolutionary models computed by Stothers (20) for $M = 45 M_\odot - 1000 M_\odot$.

The construction of models in which radiation pressure dominates gas pressure may be something of an academic exercise since Schwarzschild & Härm (21) have shown that such models are secularly unstable against radial pulsations in the linear approximation. On the other hand, there is as yet no guarantee that the pulsation amplitude will increase without limit when nonlinear terms are included, or that a star initially more massive than the stability limit might not survive for a significant fraction of its nominal main-sequence lifetime.

For all the models shown in Figure 3 with mass above $\sim 2.25 M_\odot$, the mass fraction in the convective core decreases with time as a consequence of decreasing interior opacity. In all of these stars, the major energy source is the CN cycle. For less massive stars, which possess convective cores at the beginning of the main-sequence phase, the mass fraction in the convective core increases as core temperatures and densities increase. This is because the CN-cycle contribution to energy production increases relative to the p-p chain contribution, and energy production becomes more concentrated toward the stellar center. Eventually the core mass reaches a maximum and thereafter decreases as the effect of decreasing interior opacities overwhelms the effect of the increasing central concentration of energy sources. Although no computations have yet been published to show this explicitly, it is clear that stars which possess no convective core at the start of the main-sequence phase (mass slightly less than $1.1 M_\odot$ in the present instance) may develop one as evolution progresses.

In stars more massive than about $8 M_\odot$, complications arise in the treatment of energy flow outside of the receding convective core. In several regions, matter becomes formally unstable against convection, but the extent to which mixing occurs in these regions is not clear. One approach (20, 22–25) has been to distribute composition parameters within such regions in such a way that the radiative temperature gradient equals the adiabatic tempera-

ture gradient. A satisfactory physical justification for this procedure has not been formulated.

The occurrence of an overall contraction phase (points 2 to 3 in Figure 3, where applicable) is correlated in a one-to-one fashion with the occurrence of a convective core during the period of core hydrogen burning. The occurrence of a strong shell-development stage—marked by an extremely rapid core contraction and, for not too massive stars, by a concurrent rapid cooling—is likewise tied to the presence of a relatively large convective core during the core hydrogen-burning phase. The relative magnitude of the decrease in central temperatures during the shell-development stage becomes smaller as stellar mass is increased, vanishing near $10M_{\odot}$. Beyond $10M_{\odot}$, central temperatures continue to rise following the exhaustion of central hydrogen. That central regions in sufficiently massive stars continue to heat following the exhaustion of central hydrogen is correlated with the fact that, in such stars, the mean convective-core mass exceeds the Schönberg-Chandrasekhar (S-C) limit during the phase of overall contraction.

For light stars, which do not possess a convective core while the central hydrogen abundance is finite, the phase of overall contraction is absent and the core helium-burning phase merges smoothly and uneventfully into the phase of hydrogen burning in a thick shell. The central temperature in these light stars does not drop during the shell-development stage.

The lifetime of a star in the thick-shell phase depends in an obvious way on the mean mass fraction in the convective core during the overall-contraction phase. If this mass fraction is larger than the effective S-C limit, then the thick-shell phase is quite rapid. In fact, the shell forms and narrows at the same time, while the core continues to heat as it condenses. For less massive stars, with mean convective cores smaller than the S-C limit, the lifetime in the thick-shell phase is proportional to the amount of fuel remaining, at the start of the phase, between the shell-base and the S-C limit. Since the mean mass fraction in the convective core decreases with stellar mass, the lifetime of the thick-shell phase τ_s, relative to the lifetime of the core hydrogen-burning phase τ_{HC}, increases with decreasing stellar mass. Two other factors contribute to the increase in τ_s/τ_{HC} with decreasing mass: the increasing importance of electron degeneracy, and the increasing smoothness in the variation of molecular weight with mass fraction. The additional contribution of electron degeneracy to core pressure permits the hydrogen-exhausted core to attain a larger mass prior to the onset of shell narrowing. In addition, the S-C limit is proportional to the square of the molecular weight at the hydrogen-rich outer edge of the shell (11). In the $1M_{\odot}$ model, the mass fraction in the hydrogen-exhausted core reaches $\sim$0.13 during the thick-shell phase, compared to a mass fraction of $\sim$0.10 in upper main-sequence stars with mass below $\sim 10M_{\odot}$.

When τ_s/τ_{HC} is large it makes sense to include the period of thick-shell burning as a part of the main-sequence phase. The theoretical main sequence

is then defined as the region where pure hydrogen burning occurs on a long time scale rather than as just the region where hydrogen burning occurs in the core. In terms of the model paths exhibited in Figure 3, limits to the main-sequence band may be set as follows. The high-temperature limit corresponds, of course, to the locus of points 1. For all $\log L \geq 2.0$, the low-temperature limit is obtained by joining points labeled 2. For all $\log L \leq 1.0$, the low-temperature limit is obtained by joining points 4. As a rough average, the main-sequence band is characterized by a temperature spread $\Delta(\log T_e) \sim 1.2$ at any given luminosity and a luminosity spread $\Delta(\log L) \sim 0.75$ or $\Delta M_{\text{bol}} \sim 2$ at any given surface temperature. This compares with an average spread of $\Delta(\log T_e) \sim 0.045$ at constant L, and $\Delta(\log L) \sim .3$ or $\Delta M_{\text{bol}} \sim 0.8$ at constant T_e, associated with ranges in composition variables of about $(\Delta X, \Delta Z) \sim (0.2, 0.02)$.

The appearance of the main-sequence band in the mass-luminosity plane is also of interest. The arrows within the band in Figure 4 are evolutionary tracks for models during major hydrogen-burning phases. Where two arrows occur at a given mass, the lower arrow corresponds to evolution prior to the phase of overall contraction and the upper arrow corresponds to evolution in the phase of thick-shell burning. Below $\log L \sim 0.4$ the upper limit to the main-sequence band is an estimate. The dashed curve below $\log L \sim 0.4$ in Figure 4 is an estimate of the location of low-mass stars which have been allowed to evolve for only 10^{10} yr.

To the Red-Giant Tip

In all but the lightest stars, where the mass fraction in the convective envelope is already quite large when the shell-narrowing phase begins, the strength of the shell decreases and appreciable absorption occurs in the radiative portions of the envelope as the shell narrows. It is of interest that the base of the giant branch (points 5 in Figure 3, where applicable) occurs at approximately the same surface temperature for all stars of the same composition, regardless of mass.

The most important characteristic of the shell-narrowing phase is the rapid rise in central temperatures and densities. The more massive the star and, hence, the higher the core temperatures are to start with, the earlier do the core temperatures become high enough to ignite the $N^{14} \rightarrow O^{18}$ reactions. Ignition and burning occur along the giant branch (points 5–6) in the $5M_\odot$ model. In the $9M_\odot$ model, ignition occurs in the "Hertzsprung gap" (points 4–5), leading to a rise in luminosity not found along tracks of less massive stars. In the $15M_\odot$ star, $N^{14} \rightarrow N^{18}$ reactions lead also to a brief luminosity rise (just prior to point 6). In the $3M_\odot$ star, $N^{14} \rightarrow O^{18}$ reactions force the star to *descend* along the giant branch until N^{14} is exhausted in the core, whereupon reascent commences.

A major dichotomy in the character of giant-branch evolution occurs at about $2.25M_\odot$. In stars more massive than this, core temperatures continue

to rise monotonically as the star ascends the giant branch. Helium-burning reactions commence and terminate the ascent before electron degeneracy becomes appreciable in the core.

As stars less massive than $2.25 M_\odot$ ascend the giant branch, the degree of electron degeneracy grows to significant proportions before helium-burning reactions are ignited. In all cases, central temperatures drop temporarily when the electron Fermi-energy ϵ_F becomes comparable to kT. Two effects are operating in producing this drop: The *relative* importance of electron conduction increases with increasing degeneracy. The effective opacity drops and the available thermal energy flows out more readily, tending to make the core isothermal. As the electron Fermi-energy rises, energy is required to increase the nonthermal kinetic energy of the electrons. The most readily available energy is thermal.

After near-isothermality is approached in the core, central temperatures begin to rise again, but much less rapidly than in the absence of degeneracy. The efficiency of electron conduction ensures that central temperatures rise not much more rapidly than shell temperatures. As a result, low-mass stars rise quite far above the base of the giant branch before helium-burning reactions are ignited. Before helium burning commences in such stars, the mass fraction in the nearly pure helium core far exceeds the S-C limit. This is in strong contrast with stars more massive than $2.25 M_\odot$, within which the mass fraction in the hydrogen-exhausted core, when helium burning commences, is not much larger than it was at the end of the main-sequence phase.

Mestel (26) was the first to suggest that the ignition of nuclear fuel in a region of high electron degeneracy would be explosive. Schwarzschild & Härm (27) have demonstrated this actually to be the case when helium burning commences in the degenerate core of a light star. At the peak of the "flash," energy is released by nuclear reactions at the rate of $\sim 10^{11} L_\odot$. None of this energy escapes beyond a convective core which reaches almost to the hydrogen-burning shell (27, 28). Core temperatures rise until degeneracy is lifted. After degeneracy is lifted, the core expands and cools. Thereafter helium burning continues in a manner similar to that in more massive stars. It is clear from the trends exhibited by the tracks in Figure 3 that after degeneracy has been lifted, evolutionary tracks for light Population I stars will be compressed tightly against the giant branch, at least for stellar masses $M \gtrsim M_\odot$, for which the mass in the hydrogen-exhausted core is approximately $0.4 M_\odot$ at the start of the flash phase.

The mass in the hydrogen-exhausted core at the start of the flash phase appears to be relatively independent of the abundance of elements heavier than helium and also relatively independent of the total mass outside of the degenerate core. For values of initial $X \sim 0.6$–0.7, the helium-core mass is about $0.4 M_\odot$ (3, 17). For values of $X \sim 0.9$, the helium core mass is $\sim 0.6 M_\odot$ (3, 27).

These values for critical core mass apply if it is the triple-alpha process which initiates the flash. In the core of Population I stars, most of the initial

oxygen and carbon has been converted into N^{14} which, on reacting with helium, produces energy rapidly at temperatures somewhat lower than required by the triple-alpha process. The N^{14}-flash in low-mass population models will therefore occur when the core mass is less than the critical mass for triple-alpha flashing. The difference in the brightness of the red-giant tip—depending on whether it is determined by the onset of N^{14} flashing or by the onset of triple-alpha flashing—amounts to several magnitudes (17).

The effect on giant-branch evolution of energy losses associated with the plasma-neutrino process (29, 30) has yet to be studied numerically. It is clear that plasma-neutrino losses are important (31) and may significantly alter the manner in which helium burning commences in the core of a light star. The inclusion of plasma-neutrino losses is expected to have the following effect. Energy loss will be most significant near the stellar center where densities are highest and the degree of degeneracy is greatest. On the other hand, the rate at which gravitational energy is released, as a result of the continued addition of helium to the partially degenerate core, will be larger in regions where the degree of degeneracy is smaller. Hence, in order to supply the neutrino loss from central regions, energy will tend to flow by conduction from regions away from the center (where the compression rate is large) toward the center (where the compression rate is small). The maximum in core temperatures will therefore not occur at the center but instead somewhere between the center and the shell. Helium burning will commence not at the center but in some region away from the center where the degree of degeneracy is smaller. The mass of the helium core will be larger when helium burning commences and the helium flash will be less violent than when neutrino losses are neglected—if indeed helium ignition is at all violently explosive.

Helium-Burning Phases

As may be seen from Figure 3, evolutionary tracks during core helium burning are topologically equivalent for stars in the mass range $3 \lesssim M/M_\odot \lesssim 9$. For stars in this range, several mass-dependent trends are of importance.

In the H-R diagram, the separation between the two major phases of core helium burning becomes more pronounced with increasing stellar mass. In both the $5M_\odot$ and $9M_\odot$ cases, the phase of rapid envelope contraction that is correlated with the decrease in the mass fraction of the convective envelope is bounded roughly by points 7 and 8. In the $9M_\odot$ case, the rapidity of the envelope contraction is clearly reflected by the increase in luminosity along the evolutionary track just beyond point 7. This brightening is the result of the release of gravitational energy within the contracting envelope. For stars less massive than $3M_\odot$, the phase of rapid envelope contraction is absent.

For all stars less massive than $\sim 9M_\odot$, then, the first major phase of core helium burning occurs near the giant branch (points 6 to 7), whereas the second major phase occurs (between points 8 and 9) in a region which becomes successively further removed from the giant branch as the mass in-

creases. As the mass is increased, the time spent in the second phase of core helium burning increases relative to the time spent in the first phase.

In a star of $15M_{\odot}$, the core temperatures reach high enough values immediately following the main-sequence phase for the triple-alpha reactions to be ignited, and the long-term phase of core helium burning begins before the star reaches the red-giant phase. The star spends most of the core helium-burning phase between points 6 and 8.

A core helium-burning band or main sequence for massive stars may now be defined. Its high-temperature edge joins points 9′ along the $3M_{\odot}$, $5M_{\odot}$, and $9M_{\odot}$ tracks with point 6 along the $15M_{\odot}$ track. Its low-temperature edge joins points 8 along the $15M_{\odot}$, $9M_{\odot}$, and $5M_{\odot}$ tracks with point 6 along the $3M_{\odot}$ track. Defined in this way, the core helium-burning band is roughly parallel to the hydrogen-burning main sequence and has roughly the same width. A subsidiary core helium-burning branch may be defined by joining first points 7 and then points 6 along the $(3\text{–}9)M_{\odot}$ tracks. For the models represented in Figure 3, the combined lifetime in the phases of core helium burning relative to the lifetime in the main-sequence phase decreases from about 0.3 near $3M_{\odot}$ to about 0.15 near $15M_{\odot}$.

One may consider the position in the H-R diagram of the major core helium-burning band as established only qualitatively. In contrast with the situation along the hydrogen-burning main sequence, known uncertainties in input physics make the position of this band, for any given initial composition, indeterminate by *at least* the width of the band. Further, a variation in the composition within Population I limits can alter the position of the band even more.

In particular, the luminosity at which the band strikes the line defined by the locus of red-giant tips (points 6 in Figure 3, where applicable) is highly uncertain and sensitive to composition changes. For example, calculations by Hofmeister (9) show that for the initial composition $X=0.74$, $Z=0.021$, *all* phases of helium burning are confined to the giant branch for stars at least as massive as $9M_{\odot}$. The core helium-burning band thus breaks away (if at all) from the locus of giant branches at luminosities in excess of $\log L \sim 4.0$. With an initial composition of $X=0.60$, $Z=0.044$ and the same input physics, Hofmeister finds that the core helium-burning band breaks away at $\log L \sim 2.7$.

The position in the H-R diagram of evolutionary paths during the period of helium burning in a thick shell is even more uncertain than the position of evolutionary paths during the preceding core helium-burning phase. A discussion of mass-dependent trends should therefore be deferred until the basic physical assumptions are better established and more model calculations are available. The same may be said of still more advanced phases.

COMPARISON WITH OBSERVATIONS

A quantitative comparison between model results and observational data requires, unfortunately, uncertain theoretical transformations of incomplete

observational data. The statement of observational results in terms of such quantities as L, T_e, and M is as uncertain as the structure of model stars. At present, one can only hope to establish rough consistency, or discover major discrepancies, between theory and observation.

The Main-Sequence Band

In Figure 5, the curves labeled $ZAMS_0$ and $ZAMS_1$ represent the theoretical zero-age main sequence defined by models of initial composition $(X, Y, Z) = (0.71, 0.27, 0.02)$ and $(l_{\text{mix}}/\text{H}_{\text{dens}}) = 0.5$, when the effect of line absorption on opacity is and is not neglected (13).

The curve labeled $TAMS$ represents the theoretical termination of the main-sequence phase as defined in the previous section, again with line absorption neglected. The dashed curve labeled overall contraction is the locus of models which are beginning the phase of overall contraction while hydrogen is burning in a convective core.

The crosses in Figure 5 mark the position of the standard zero-age main sequence, as defined by stars in the Hyades, the Pleiades, and NGC 2362. It is assumed that composition differences between the clusters may be neglected and that distances to Hyades cluster stars, as determined by the convergent-point method, are correct. Observational data and the conversion from $B-V$ and M_v to $\log T_e$ and $\log L$ are taken for most stars from Sandage (32). The ranges over which the cluster diagrams are forced to coincide are indicated along the left-hand portion of Figure 5.

Considering all of the uncertainties, the fit between the theoretical and the standard $ZAMS$ would appear to be remarkably good. However, comparisons in the mass-luminosity plane suggest that this agreement may be misleading.

In Figure 6, the theoretical main-sequence band for models of composition $(X, Y, Z) = (0.71, 0.27, 0.02)$ is bounded by the curves labeled $ZAMS$ and $TAMS$. The curve labeled $GAMS$ is an estimated locus of model stars which have evolved for 10^{10} years. For a galactic age of $\sim 10^{10}$ yr, the upper limit to the main-sequence band for the chosen composition should thus be the curve $GAMS$. The crosses denote the position of nearby main-sequence band stars selected by Schwarzschild (1).

Below $\log L \sim 2$, the *shape* of the theoretical main-sequence band agrees very nicely with the shape of the band defined by nearby stars. Deviations at very low luminosity could be due to inaccurate bolometric corrections. Since the models of very low luminosity are completely convective below the photosphere, their luminosity is very sensitive to changes in photospheric opacity. Hence, an equally likely explanation of the deviation is that the surface opacities are overestimated.

Above $\log L \sim 3$, the "empirical" main-sequence band falls consistently below the theoretical band. This deviation could also be attributed to an underestimate of bolometric corrections. It cannot easily be accounted for by

a variation of composition with stellar mass and it is unlikely that faulty opacities can be blamed.

The squares in Figure 6 represent the position of components of several binaries in the Hyades cluster, again assuming that the convergent-point method of obtaining distance is applicable. Data are from Eggen (33) as treated by Iben (13). In order to simplify the discussion, a point characterized by $\log L = 0.0$, $\log M = -0.15$ shall be taken as representative of the Hyades cluster stars for which masses have been estimated.

It has been shown (13) that for a choice of Z in the range 0.01 to 0.04, the initial hydrogen abundance required to reproduce the representative point in the mass-luminosity plane obeys the relationship $X \simeq .5 - 4.65(Z - .01)$. Adherence to this relationship has the distressing consequence that for reasonable values of (Z/X), it is impossible to achieve consistency in the H-R diagram between models and the standard $ZAMS$ (13, 34). It has been suggested (13) that consistency may be achieved by giving up the assumption that Pleiades stars have the same composition as Hyades stars.

Hodge & Wallerstein (35) and Faulkner & Stefensen (36) have suggested that the convergent-point method of determining the distance to individual members of the Hyades cluster may be inapplicable, as it would be if the cluster were expanding or rotating. Hodge & Wallerstein conclude that the currently adopted distance modulus for the Hyades may be an underestimate. They point out that by increasing the distance modulus, much of the difficulty in achieving consistency between models and the observations in both the H-R and M-L planes is removed.

It is worth while to examine in some detail how this comes about. The total mass derived for a binary system is proportional to the cube of the adopted distance to the binary, whereas the luminosity is proportional to the square of the adopted distance. Hence a change in the adopted distance alters the position of a component star in the M-L diagram by $\Delta(\log M) = 3\Delta(\log d) = \frac{3}{2}\Delta(\log L)$, where d is the adopted distance. An increase of $\Delta(\log d) = 0.067$ brings the standard Hyades star, initially at $\log M = -0.15$, $\log L = 0.0$,

---

FIG. 5. Theoretical predictions in the Hertzsprung-Russell diagram. Units are the same as in Figure 3. The curves labeled $ZAMS_0$ and $TAMS_0$ represent the theoretical boundaries of the main-sequence band, as defined in the text, for the composition $(X,Y,Z) = (0.71, 0.27, 0.02)$, when line effects are omitted. The curve $ZAMS_1$ is the estimated position of the zero-age main sequence when line effects are included. Crosses define the standard $ZAMS$ as determined by stars in the Hyades, Pleiades, and NGC 2362. The lines and vectors in the lower left-hand portion of the Figure describe possible effects of rotation on homogeneous model stars. Theoretical estimates for the core helium-burning bands and the position of the Cepheid instability strip are also shown.

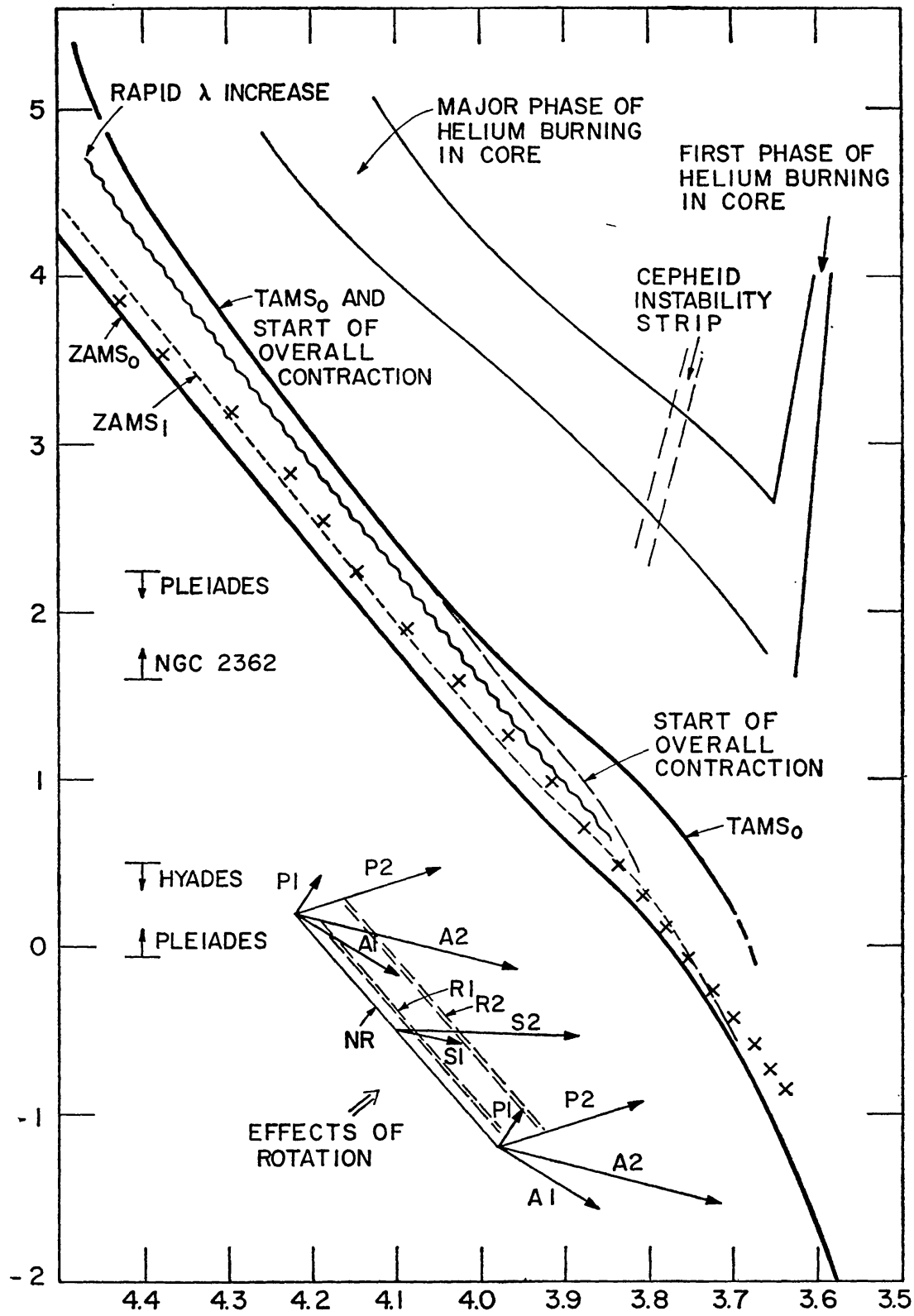

precisely onto the model *ZAMS* in the *M-L* plane for the composition (X, Y, Z) = (0.71, 0.27, 0.02). This change is indicated by the arrow in Figure 6.

In the H-R diagram, the standard *ZAMS* must now be raised by $\Delta(\log L) = 0.133$, and it will be necessary to alter the model composition in order to achieve consistency again between models and the observations. The required composition change must not be such as to destroy the fit in the mass-luminosity plane.

Since the value of (l/H) may be adjusted to achieve a fit along the lower main sequence, a fit in the H-R diagram should be sought only along the upper main sequence. In the neighborhood of $\log T_e = 4.1$–4.2, one has that $\Delta(\log L) = -(0.66\Delta X + 10.5\Delta Z)$, when $\log T_e = \text{const}$. In the *M-L* plane, for $\log M = 0.0$, and $X = 0.6$–0.7, the position of a star will not change if $\Delta Z \simeq -0.19\Delta X$. Thus we require that $-(0.66 - 10.5 \times 0.19)\Delta X = -1.34\Delta X = \Delta(\log L)$ or $\Delta X = -0.75\Delta(\log L)$, and $\Delta Z = 0.142\Delta(\log L)$. Inserting $\Delta(\log L) = 0.133$, we find that $\Delta X \sim -0.1$, $\Delta Z \sim 0.019$ and that the mean composition of stars along the *modified* standard *ZAMS* is $(X, Y, Z) \sim (0.61, 0.35, 0.04)$. Thus, consistency in both the H-R and *M-L* planes can be achieved fairly easily by increasing the adopted distance to each Hyades star by about 17 per cent.

A value of $(Z/X)_{\text{Hy}} \sim 0.064$ is perhaps uncomfortably large compared to $(Z/X) \sim 0.028$ [$= (Z/X)_\odot$?]. One possible solution is that the effect of including line absorption has been underestimated. On the other hand, the value of $(Z/X)_\odot$ cannot be considered to be established to better than perhaps 50 per cent.

The curve labeled Hyades group in Figure 6 is a rough mean for stars in the Hyades group as obtained by Eggen (37, 38) using the convergent-point method to determine distance. Between $\log L = 1.0$ and $\log L = 1.4$, the slope of the group *M-L* relationship is $[\Delta(\log L)/\Delta(\log M)] \sim 0.8$, whereas the theoretical slope over this range is ~ 4.0. The group slope cannot be accounted for theoretically by assuming that the hydrogen abundance increases with mass in this range and it is unlikely that rotation effects (rotation rate or aspect angle increasing with mass) can be responsible for the discrepancy. The magnitude of the discrepancy between the group result and theory

FIG. 6. Comparison between theory and the observations in the mass-luminosity plane. Units are the same as in Figure 4. The curves *ZAMS* and *TAMS* represent the theoretical boundaries of the main-sequence band, as defined in the text. The curve *GAMS* is an estimated locus of low-mass models which have evolved for 10^{10} yr. Crosses represent observational results for nearby stars, and boxes correspond to stars in the Hyades cluster. The dashed line represents results for the Hyades group.

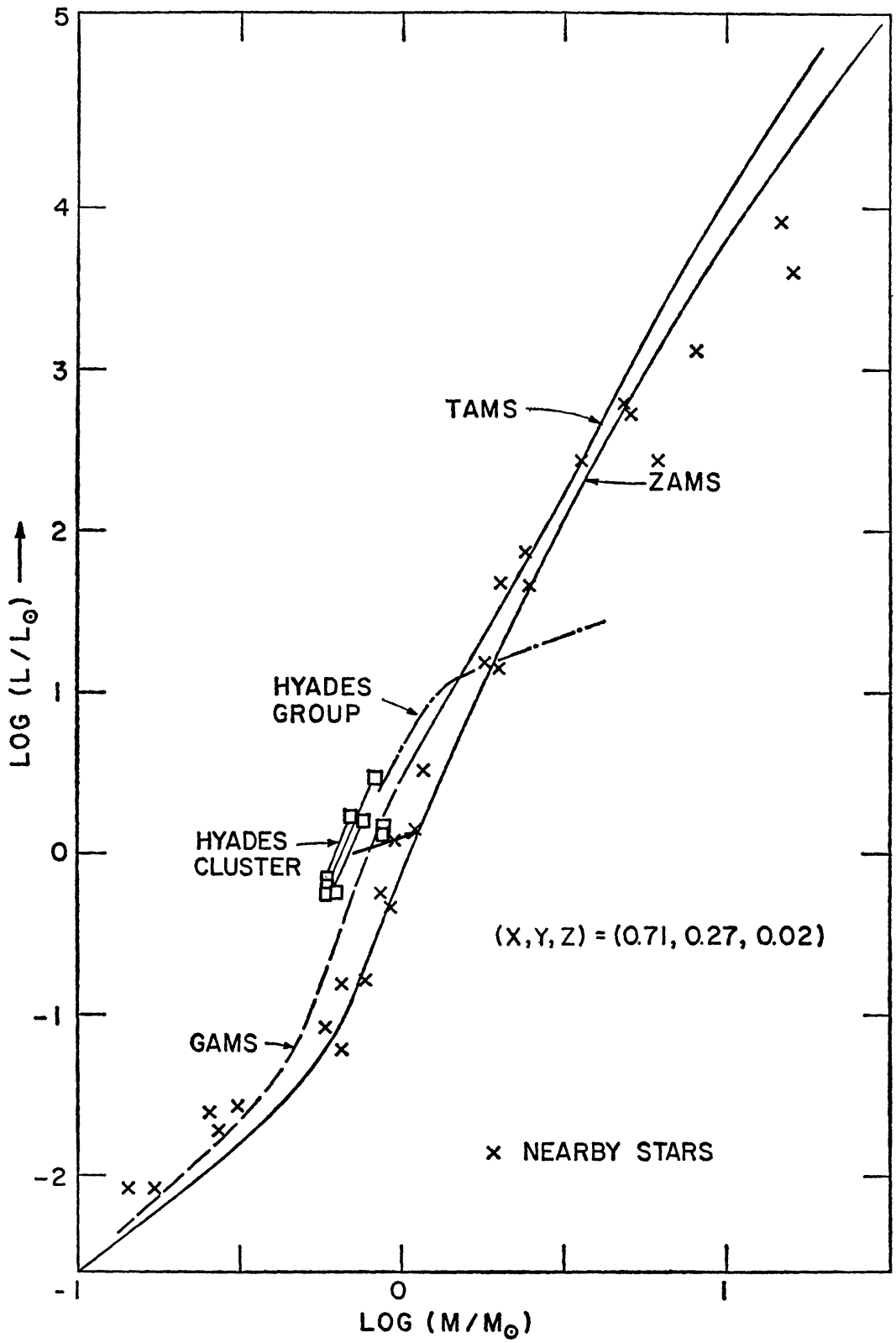

casts further doubt upon the applicability of the convergent-point method in obtaining distances to members of the Hyades group.

Effects of Rotation and "Be" Stars

Rotational effects have stimulated considerable recent work, both theoretical (39–43) and observational (44–47). Since the effects of rotation on stellar structure and on observable properties are sensitive to as yet uncertain theoretical assumptions and simplifications, it is useful to have a strong interplay between theoretical suggestions and the observations.

Of primary interest here is a recent analysis by Strittmatter (47). From a study of the relationship between M_v and $|V \sin i|$ for stars in the Praesepe cluster, Strittmatter finds that at a given color, rotating stars are displaced in magnitude above an arbitrary zero-age main sequence for nonrotating stars by an amount proportional to $|V \sin i|^2$. This is to be expected from the first-order theoretical treatments given by Sweet & Roy (48) and by Roxburgh & Strittmatter (49).

The dependence of ΔM_{bol} and $\Delta(\log T_e)$ on the parameter $\lambda = V_e^2/(GM/R)$ = (equatorial velocity)^2/(surface gravitational potential) is given in Table V for two different sets of assumptions. In Figure 5, the vectors $P1$ and $P2$ represent the displacement as predicted by the two theories for a star viewed pole-on when $\lambda = 1$. The vectors $A1$ and $A2$ represent the predicted displacement for $\lambda = 1$ when the star is viewed equator-on. The vectors $S1$ and $S2$ are estimated displacements for $\lambda = 1$ after an average over aspect angle has been performed.

The line in Figure 5 labeled NR is an arbitrarily placed zero-age main sequence for nonrotating stars. The dashed lines labeled $R1$ and $R2$ represent the displaced positions of the $ZAMS$ for rotating stars predicted by the two theories when $\lambda = \frac{1}{3}$ (for all stars).

It is significant that the displacement of the $ZAMS$ is relatively insensitive to aspect angle. According to the two theories, $\Delta(\log L)_1 \sim 0.33\lambda$ or $\Delta(\log L)_2 \sim 1.28\lambda$ when T_e = const; and $\Delta(\log T_e)_1 \sim -0.066\lambda$ or $\Delta(\log T_e)_2 \sim -0.224\lambda$ when L = const. Rotation thus introduces an additional spread into the main-sequence band comparable to that due to differences in composition and perhaps even to that due to evolution. Note that the luminosity of a single "average" star (averaged over aspect angle) is lowered by an insignificant amount for a reasonable rotation parameter (see the intersection of the curves NR, $R1$, and $R2$ with the vectors $S1$ and $S2$). Thus, rotation affects the position of a group of stars in the M-L plane much less than their position in the H-R diagram.

The effect of rotation on the standard $ZAMS$ is minimized by the fact that the lower envelope (rather than the mean) of the main-sequence band is emphasized in determining the $ZAMS$. Further, the fact that the shape of the observational $ZAMS$ is in fair agreement with that predicted on the basis of nonrotating models argues against a significant rotational effect.

The effect of rotation on evolutionary tracks has not yet been investi-

TABLE V

CHANGES IN BOLOMETRIC MAGNITUDE AND EFFECTIVE TEMPERATURE DUE TO ROTATION

Model	Pole-on		Axis-on	
	$\Delta M_{bol}/\lambda$	$\Delta \log_{10} T_e/\lambda$	$\Delta M_{bol}/\lambda$	$\Delta \log_{10} T_e/\lambda$
Uniformly rotating star with circulation Sweet & Roy (1953)	−0.552	−0.0286	+0.928	−0.1208
Rotating magnetic star, zero field in core Roxburgh & Strittmatter (1966)	−0.662	−0.168	+0.849	−0.262

gated quantitatively. It is nevertheless interesting to discuss the question qualitatively. For simplicity, let us suppose that the position in the H-R diagram of a rotating star is displaced from that of a nonrotating star of the same age by a vector whose direction is constant but whose magnitude is proportional to the quantity $\lambda = V_e^2 R/GM$. Let us further suppose, again for simplicity, that the star rotates as a rigid body and that angular momentum is conserved. For each nonrotating model in an evolutionary sequence, the quantity R^3/I^2, where R is the radius and I is the solid-body moment of inertia, can be calculated. If the corresponding rotating model has an angular momentum J, then we can estimate $\lambda = (J^2/GM)\ (R^3/I^2)$.

In Figure 7, the time dependence of λ for the $1.25 M_\odot$ model depicted in Figure 3 is compared with several other $1.25 M_\odot$ characteristics. The value of J^2 is chosen in such a way that $\lambda_{max} \simeq 0.96$. Note that λ increases steadily throughout the phase of core hydrogen burning and also throughout the phase of hydrogen burning in a thick shell. The parameter λ increases most rapidly near the end of the phase of overall contraction, at the same time that the central temperature drops and core contraction is particularly rapid; it does not begin to decrease until near the end of the phase of hydrogen burning in a thick shell. As the star evolves toward the giant branch, λ drops rapidly and attains negligible size along the giant branch. Thus, if $J =$ const, rotational effects are expected to increase monotonically as the star evolves off the main sequence through most of the thick-shell stage and then to become much less important during the giant stage.

During phases of pure hydrogen burning, the relationship between changes in λ and variations in interior characteristics is much the same for all model stars with mass $M \geq 1.25 M_\odot$. In all cases, λ increases throughout the main-sequence phase and during most of the thick-shell phase. The most rapid rate of increase in λ occurs toward the end of the phase of overall con-

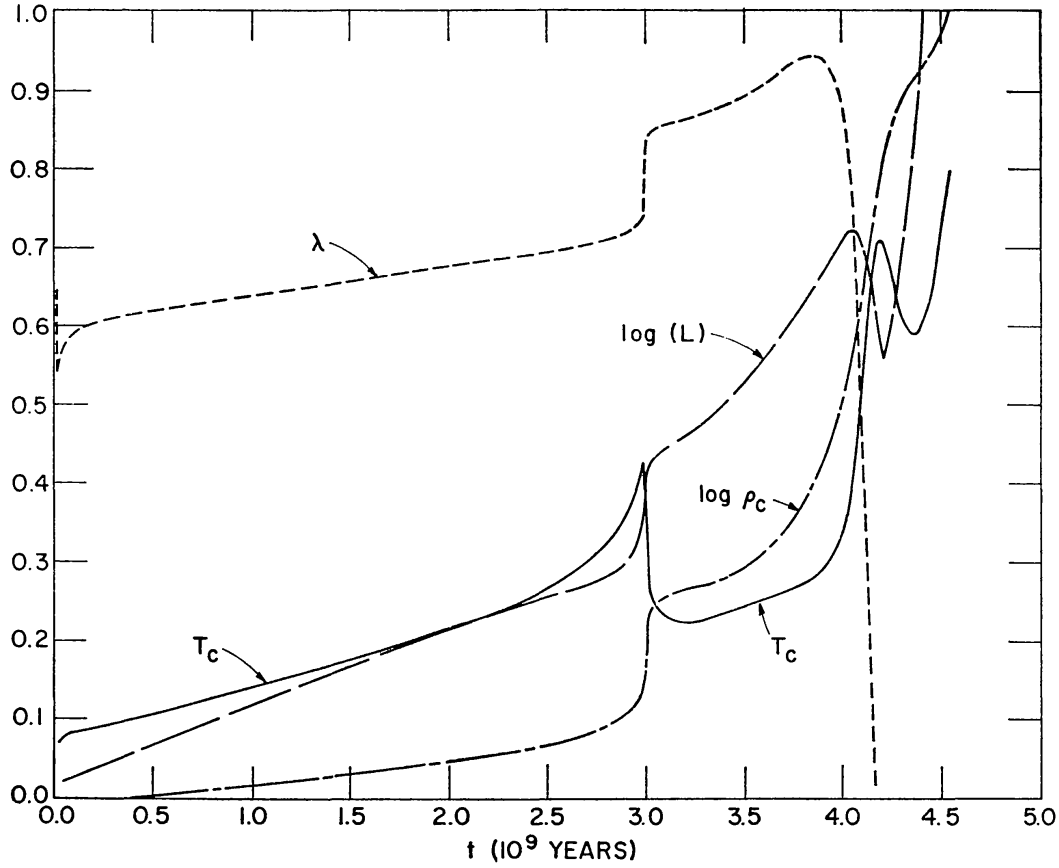

FIG. 7. The time dependences of the rotation parameter $\lambda = \text{const} \times (R^3/I^2)$, luminosity, central temperature, and central density for the $1.25 M_\odot$ model described in Figure 3. Here R and I represent the stellar radius and the moment of inertia. Luminosity is in solar units and temperature and density are in deg K and g/cm^3, respectively. Scale limits correspond to $0 \leq \lambda \leq 1$, $0.35 \leq \log L \leq 0.975$, $15 \leq T_c \leq 35$, and $2.0 \leq \log \rho_c < 5.125$.

traction, and λ becomes quite small during the giant-branch phase. However, during the descent from the red-giant tip and during most of the phase of helium burning in the core, λ again increases.

A possible effect of rotation on the evolutionary track of a $3 M_\odot$ star is sketched in Figure 8. The slope of the adopted displacement vector is $d(\log L)/d(\log T_e) \simeq +0.60$ and its magnitude is proportional to λ. The slope of the displacement vector and its magnitude for $\lambda = 1$ are somewhat arbitrary choices, but are consistent with the vectors in Figure 5, labeled $S1$ and $S2$, which represent an average over aspect angle.

The speculation pictured in Figure 8 is not to be taken too seriously. A real star probably does not rotate even approximately like a rigid body (39) and the assertion that the effect of rotation on observable properties of an evolving star is proportional to the parameter λ, as determined from R^3/I^2 for nonrotating models, can at best be only a rough approximation. Further,

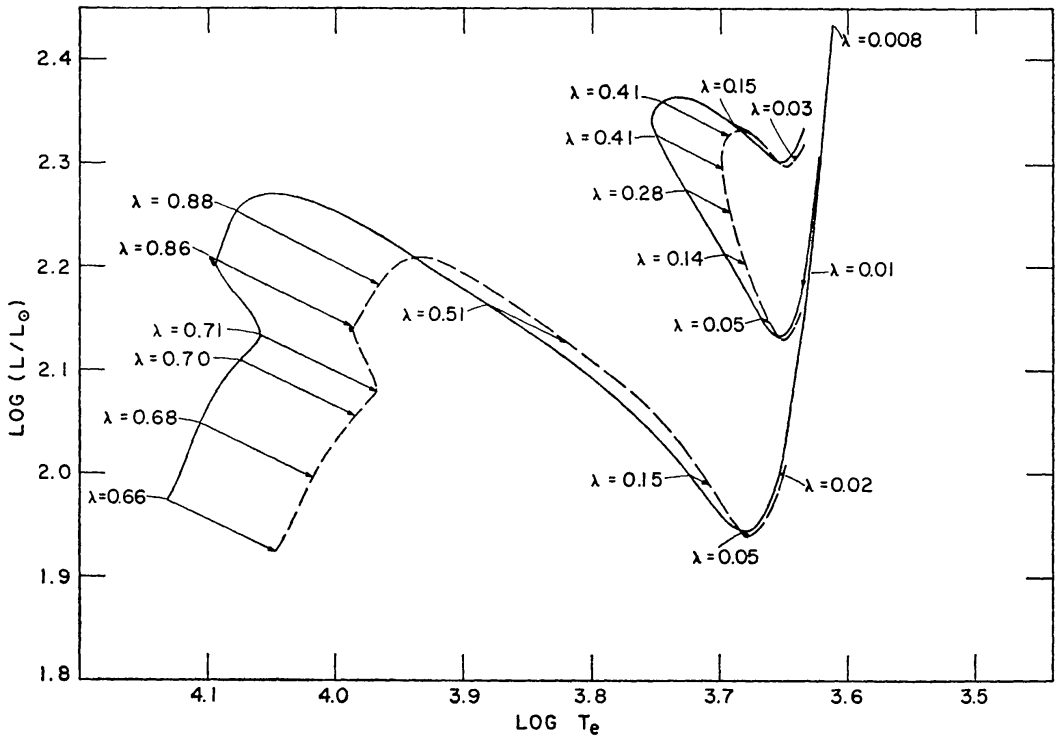

FIG. 8. A qualitative estimate of the effect of rotation on the evolutionary path of a $3M_{\odot}$ model if mass loss and angular momentum loss are neglected. The rotating model is assumed to be displaced by a vector which is proportional to the rotation parameter λ calculated for the nonrotating model. The direction of the displacement vector is constant and appropriate for some intermediate-aspect angle.

the assumption that total angular momentum (and also total mass) remains constant, even to first order, is undoubtedly wrong. In particular, if the star passes through the "Be" phase to be discussed shortly, angular momentum is probably transmitted to escaping matter through the intermediary of the magnetic field. Further, during phases characterized by a low surface temperature, when convective turbulence near the surface is particularly violent, mass loss and, concomitantly, a rapid loss of angular momentum from the star might be expected (50–52).

Crampin & Hoyle (53) were the first to attempt an explanation of Be stars in terms of the properties of calculated evolutionary models. They suggested that equatorial mass loss might occur when the parameter λ exceeds 1. Schmidt-Kaler (54) has found that extreme Be stars lie along a fairly narrow strip in the H-R diagram *parallel* to, but *above* the zero-age main sequence, and suggests that these stars are in the phase of rapidly increasing λ during or following (or both) the phase of overall contraction. Schild (55) has discussed the Be stars in h and χ Persei. He finds that extreme Be stars lie in a narrow strip lying above the *ZAMS*, but that ordinary Be stars occupy a very broad region ranging from the *ZAMS* through the region of extreme Be stars, and considerably beyond.

On the basis of the reasoning of Crampin & Hoyle, the fact that Be stars lie above the *ZAMS* is obvious from the theoretical prediction that all rotating stars lie above the *ZAMS* for nonrotating stars. The fact that ordinary Be stars cover a broad range is consistent with the fact that the parameter λ increases during most of the pure hydrogen-burning phases prior to shell narrowing. The fact that extreme Be stars lie within a very narrow band is consistent with the fact that the most rapid increase in the parameter λ, and hence the most rapid rate of predicted equatorial mass loss, occurs near the end of the phase of overall contraction. The line labeled rapid λ increase in Figure 5 marks the end of the overall contraction phase for nonrotating stars and hence marks the predicted position of extreme Be stars if rotation did not displace the position of a star in the H-R diagram. Note that this line is essentially parallel to the *ZAMS*. Introducing the predicted displacement due to rotation, we see that the extreme Be stars still lie in a narrow strip, parallel to the *ZAMS*, but considerably above it, just as found by Schmidt-Kaler and Schild.

Cepheids and Young Clusters

Cepheid statistics.—Perhaps the most exciting recent development associated with studies of relatively massive stars has been the fairly secure identification of classical Cepheids as stars in helium-burning phases (56–58, 9, 10, 51).

An understanding of two statistical properties of galactic Cepheids—the existence of a rough period-luminosity relationship and the existence of a maximum in the distribution of Cepheid numbers versus luminosity—has been obtained on the basis of studies of envelope pulsation in conjunction with studies of stellar evolution through helium-burning phases. For a recent review of theoretical results concerning pulsation, see Christy (59).

The occurrence of large-amplitude pulsation is correlated with an extensive radiative region over which opacity increases with increasing temperature. In stellar envelopes of Population I composition, the region of partial helium ionization is the seat of the driving mechanism for large-amplitude pulsation.

For a given composition, and given interior mass, instability against radial pulsation is found to occur for values of mean luminosity and mean surface temperature which lie within a fairly narrow strip in the H-R diagram. A typical instability strip is sketched in Figure 5. Keeping stellar mass fixed, as luminosity is increased within the instability strip along a line parallel to the strip, one finds the pulsation period to increase.

It is clear that the existence of a very tight period-luminosity relationship would be predicted if most stars which evolve slowly through the instability strip were of similar mass and composition, or if a fairly close correlation existed between increasing mass and increasing luminosity. In the second case, the instability strip would show more curvature than in Figure 5, being constructed of segments appropriate for stars of different mass.

An inspection of the evolutionary tracks in Figure 3 reveals that during comparable phases, there is indeed a fairly tight correlation between mass and luminosity for stars of a given composition. In particular, this is true for stars in the major phase of helium burning in the core.

The region within which models spend most of their time during core helium burning is sketched in Figure 5. The intersection between the major helium-burning band and the instability strip represents the region where most Cepheids of the chosen composition are expected to be found. Not only does the mean mass of evolving models increase with luminosity along this intersection, but the variation of stellar mass over the intersection is relatively small ($\Delta M/M \sim 1/3$). Thus, on two counts, theory suggests a relatively tight correlation between period and luminosity, as observed not only for galactic Cepheids, but for Cepheids in M31 and in the Large and Small Magellanic Clouds.

In addition, it is evident that in the distribution of Cepheid numbers versus luminosity, there should be a maximum at some luminosity within the region of intersection between the instability strip and the major helium-burning band. The predicted low-luminosity cutoff to the distribution is due to the fact that for sufficiently light stars, the maximum extension to the blue during core helium burning does not reach the instability strip. The predicted decrease in Cepheid numbers at high luminosities is due in part to the fact that sufficiently massive stars pass rapidly through the instability strip during the phase of envelope contraction separating the two major phases of core helium burning and in part to the fact that the frequency of stars in selected mass intervals is a rapidly decreasing function of the mean mass characterizing that interval.

The maximum in the distribution is predicted (10) to occur at a luminosity appropriate to that model star which, at its furthest extension to the blue, just reaches the high-temperature edge of the instability strip. The *qualitative* accord between prediction and the distribution (in numbers versus luminosity) of Cepheids in selected fields has been demonstrated by several authors (9, 10, 51).

It does not seem reasonable to attempt a more quantitative comparison at the present time. The position of the major helium-burning band is extremely sensitive to composition changes and to variations in the input physics. The position of the theoretical instability strip is also affected by changes in composition and input physics. Further, additional crossings of the instability strip on a long time scale may be associated with the phase of helium burning in a thick shell. The exact nature of these later crossings is even more uncertain than is the nature of all previous crossings.

NGC 1866.—An extremely beautiful qualitative confirmation of the general features of evolution during phases of helium burning is afforded by stars in the cluster NGC 1866. The distribution of these stars in the color-magnitude diagram, Figure 9, is taken from Arp (58). The crosses mark the mean positions of Cepheids. The smooth curve in Figure 9 is an eye-fitted mean

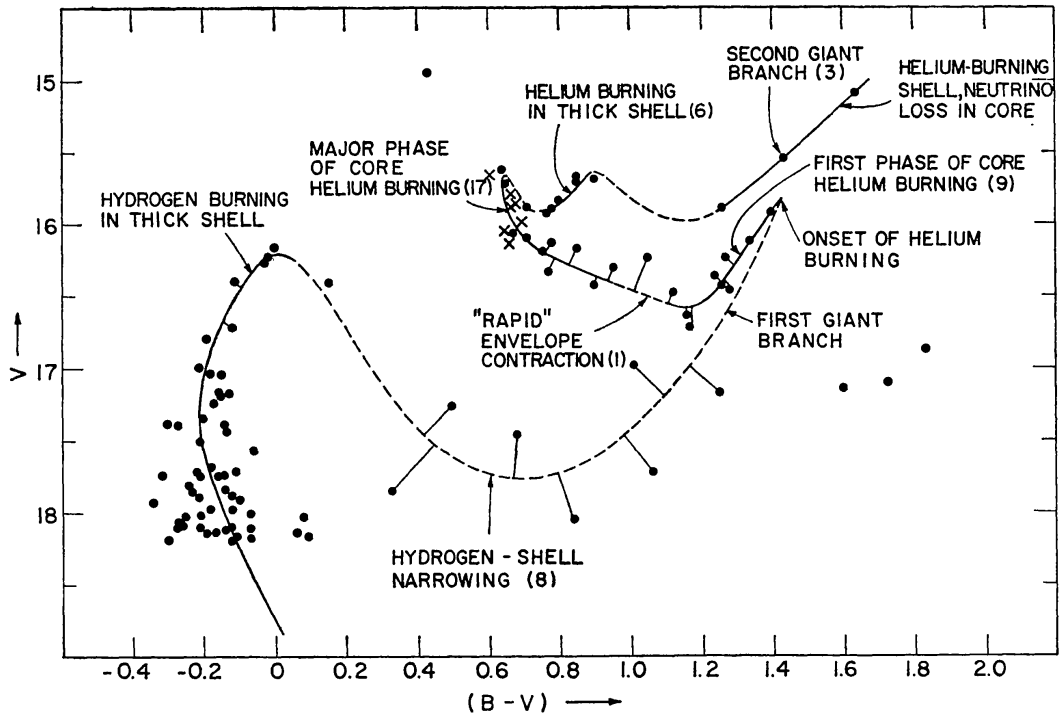

FIG. 9. The position, in the color-magnitude diagram, of stars in NGC 1866. The solid points are taken from Arp (58) and the smooth curves represent an eye-fitted mean cluster locus. Crosses denote the location of Cepheids.

cluster locus. Dashed portions along this curve represent suggested phases of rapid evolution (rapid relative to adjacent phases). Solid lines joining points to the mean curve indicate that portion of the mean curve with which each star has been identified.

The choice for the mean cluster locus in Figure 9 has been strongly influenced by the characteristics of evolutionary models in the neighborhood of $5M_{\odot}$, the mass thought by Arp to be most consistent with the luminosity level near the turnoff region of NGC 1866. The type of judgment employed is evidenced by the labels describing segments of the chosen mean curve.

Comparison with model results is essential to disentangle segments of the cluster locus near the red end of the color-magnitude diagram. For example, model results indicate that the rate of descent from the red-giant tip following the onset of helium burning in the core should be at least ten times slower than the rate of the preceding ascent. Hence, most of the stars near the first giant branch should be descending. The three stars along the segment labeled second giant branch have been associated with a phase more advanced than core helium burning. Otherwise, these three stars would suggest that helium burning begins in the core at a luminosity $\sim$1 mag brighter than predicted by current evolutionary models of mass near $5M_{\odot}$.

According to the identifications made in Figure 9, there are twice as many stars in the major phase of core helium burning as there are in the first phase.

This ratio compares quite favorably with a ratio of about 5 to 3 suggested by the $5M_\odot$ model evolution described earlier and thereby strengthens the adopted assignment of stars to the first phase of core helium burning.

Six stars are assigned to the phase of helium burning in a thick shell. That these stars are not in the core helium-burning phase is suggested by the model result that the evolution to the red which occurs near the end of the phase of core helium burning is much more rapid than the preceding evolution to the blue. The assignment of the six stars to the phase of thick-shell burning is consequently quite probable and we thus have the very useful empirical result that for a $5M_\odot$ star, the phase of helium burning in a thick shell lasts about one-fifth as long as does the preceding phase of core helium burning.

The three stars assigned to the second giant branch are probably burning helium in a thin shell, following a rapid phase of helium-shell narrowing. The *relatively* high frequency of stars along this second giant branch can be considered as supporting evidence for Weigert's result (7) that neutrino losses in the core act as a refrigerant and may prolong the phase of pure shell burning.

One disturbing feature of the star distribution in Figure 9 diminishes somewhat the confidence one can place in arguments which depend on the relative density of stars along the mean cluster locus. The fact that there are so many (eight) stars along the dashed curve in Figure 9 between the segment labeled hydrogen burning in a thick shell and the point labeled onset of helium burning is in clear conflict with evolutionary theory. The $5M_\odot$ model spends five times as long in the first phase of core helium burning (points 7 to 8 in Figure 1) as it does in the shell-narrowing and ascending-giant phases combined (points 5 to 7 in Figure 1). There are thus at least four times as many stars along the lowest dashed curve in Figure 9 as theory predicts. No theoretical explanation (other than the occurrence of additional nuclear burning processes) for this rather serious discrepancy can be offered.

h and χ Persei.—Another highly interesting distribution in the color-magnitude diagram is presented by the stars in h and χ Persei. The distribution in Figure 10 is taken from Wildey (60). It is apparent (3, 61) that the majority of stars in h and χ Persei are quite young and that most of the stars to the red of the main-sequence band below $M_v \sim -3$ are contracting onto the main sequence. Because of the dense population all along the main sequence, it is further clear that star formation has occurred continuously over a period of at least 10^7 yr. This lower limit to the age is based on the fact that the main-sequence band is populated down to at least $M_v \sim +3.5$ (61). The existence of the most luminous blue stars near the main sequence is additional support for the view that star formation has been continuous. These luminous stars may be gauged to have masses of $45–60M_\odot$, and the main-sequence lifetime for such stars is (3–4) $\times 10^6$ yr (20).

Hayashi & Cameron (62) have suggested that the red supergiants circled in Figure 10 are in a phase of evolution more advanced than that of helium burning in the core. They argue that these stars each have a mass of $15–16M_\odot$. By comparing the number of red supergiants with the number of

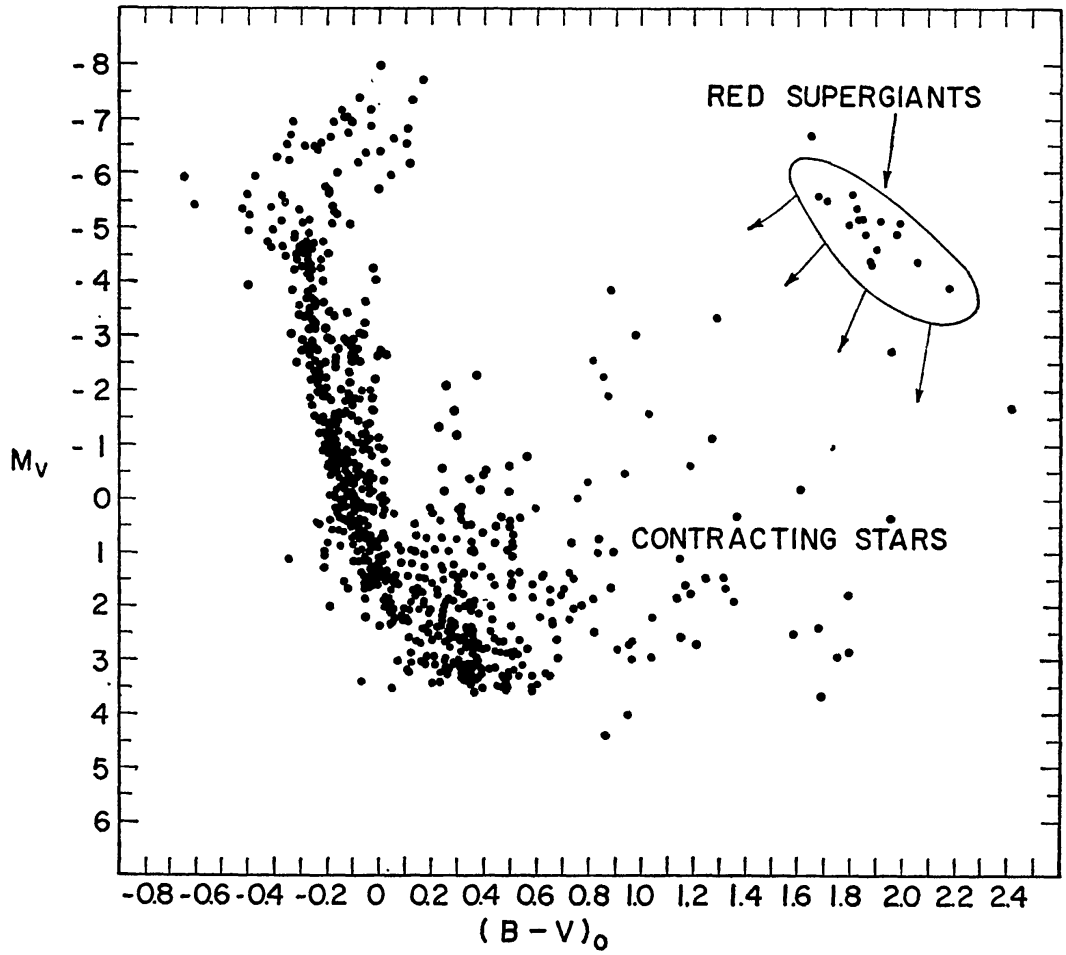

FIG. 10. The position, in the color-magnitude diagram, of stars in h and χ Persei. This Figure is reproduced from Wildey (60), except for the comments.

selected stars near the main sequence which they identify as 15–16$M_\odot$ stars in the phase of core helium burning, they conclude that the lifetime of 15–16$M_\odot$ stars in stages more advanced than core helium burning is comparable to the lifetime in the core helium-burning phase. On the basis of estimates, they then contend that model calculations for more advanced phases will give a total lifetime for these phases in accord with their interpretation of the observations, but only when neutrino loss from the core by the photoneutrino and pair annihilation processes is omitted. Objections can be raised concerning the interpretation of the observations and concerning the theory on which these conclusions are based. For example, neutrino loss from the stellar core may prolong the lifetime of relatively massive stars along the giant branch during the phase of combined hydrogen- and helium-shell burning (15). The red supergiants in h and χ Persei might be stars in a double-shell burning stage. The identification of stars near the upper main sequence in h and χ Persei (the early supergiant branch) as stars in the core helium-burning stage is also debatable. Variations in composition can shift the posi-

tion of the core helium-burning phase radically in the H-R diagram. For example, an increase in initial X and/or in Z within Population I limits may shift the evolutionary track of a $15M_{\odot}$ star during this phase from the region between points 6 and 8 in Figure 3 over to the giant branch, near point 10 in Figure 3. Thus, the red supergiants might easily be stars in the core helium-burning phase.

The identification of the red supergiants in h and χ Persei as highly evolved stars and the supposition that luminous blue stars are all evolving away from the main sequence can also be questioned. The weight of evidence suggests that stars in h and χ Persei are very young, that star formation has occurred continuously, perhaps in spurts, and that it is impossible to tell in which direction stars are evolving near the main sequence. An alternate interpretation of the red supergiants is that they are the most recently formed stars in h and χ Persei, that they have masses which cover a large range, and that they are evolving downward and to the left in the color-magnitude diagram during the pre-main-sequence phase of gravitational contraction. No conflict with theory then remains.

Old Population I Clusters

Schematic cluster loci for stars in M67 and NGC 188 are shown in Figure 11. These loci are based on data from Sandage (63) and from Johnson & Sandage (64) as treated by Iben (16). The two cluster loci have been forced to fit near the lower portion of the diagram.

When the cluster loci in Figure 11 are compared with the evolutionary tracks in Figure 3, it is obvious that stars in NGC 188 are older than stars in M67. Four major differences between the two cluster loci confirm this age separation and provide evidence in support of several mass-dependent trends predicted by the evolutionary calculations.

The most obvious difference is that in the region between the main-sequence band and the red-giant branches (points D to E and F to G), stars in M67 are more luminous than stars in NGC 188. This means, of course, that stars in M67 which have just left the main-sequence band are more massive and hence younger than the corresponding stars in NGC 188.

The existence of a gap (between points B and C) in the M67 locus suggests that stars near point C have almost the same mass as stars near point B and that evolution between points B and C is quite rapid relative to the rates of evolution toward point B and away from point C. One may conclude that all stars in M67 near and beyond point B possessed convective cores during the main-sequence phase, that stars near point B are just beginning the phase of overall contraction, and that stars near point C have begun to burn hydrogen in a thick shell. The apparent absence of a gap in the NGC 188 locus suggests that highly evolved stars in NGC 188 are too light to have possessed a convective core during the main-sequence phase. Once again, we conclude that the most massive visible stars in NGC 188 must be lighter and hence older than the most massive stars in M67.

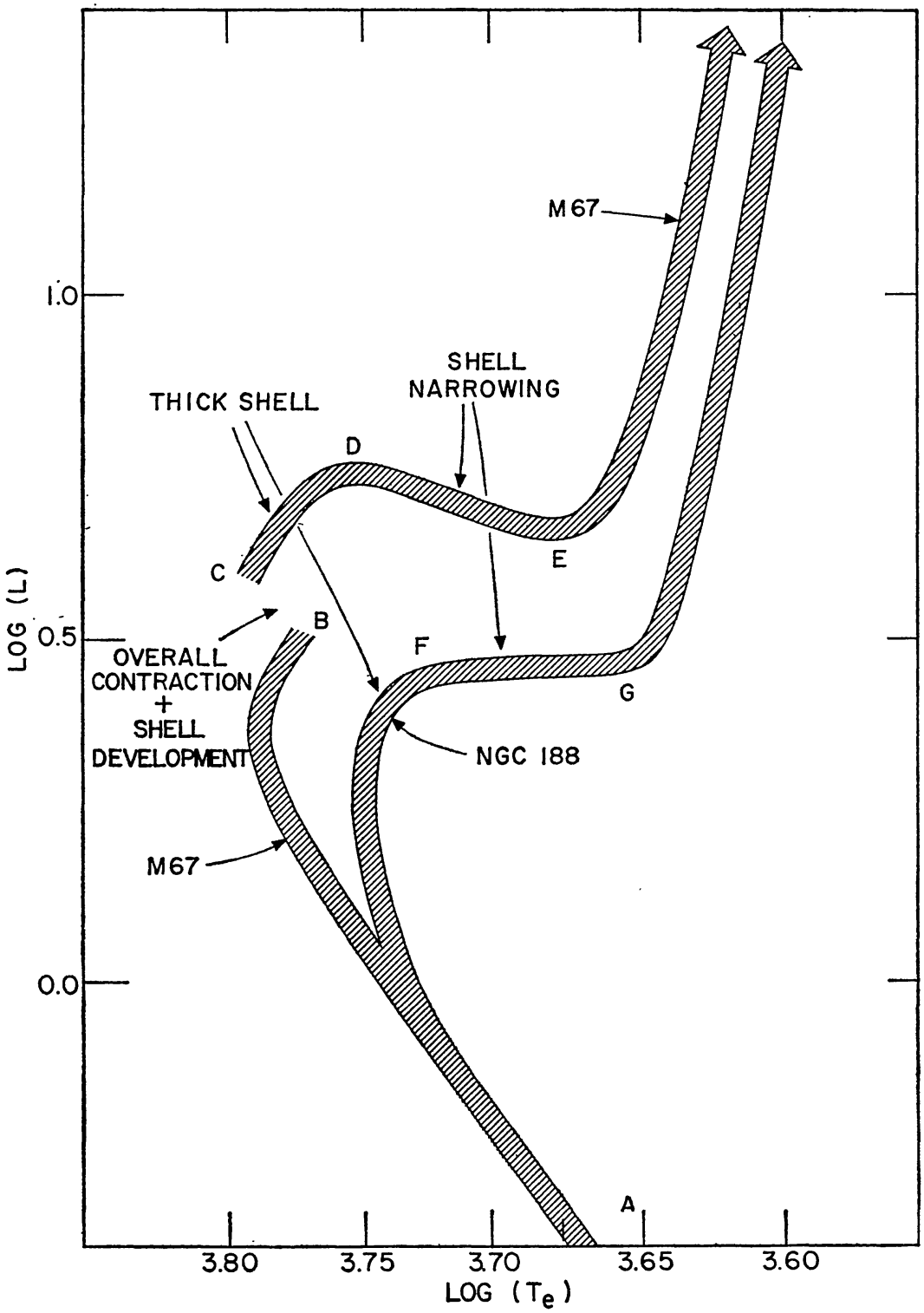

FIG. 11. Schematic cluster loci for stars in the clusters M67 and NGC 188.

The slope of the cluster locus for M67 between points D and E is steeper than that for NGC 188 between points F and G. From the tracks in Figure 3 it may be seen that as mass is decreased below $3M_{\odot}$, the luminosity drop during the shell-narrowing phase becomes less and less pronounced. This feature is reflected also in time-constant loci: the older the cluster, the lighter are the stars in the shell-narrowing phase and hence the shallower is the slope of that segment of the time-constant locus made up of stars in the shell-narrowing phase.

Finally, at a given luminosity, the giant branch of the M67 locus is distinctly bluer than is the giant branch of the NGC 188 locus. Inspection of Figure 3 shows that at a given luminosity, the giant branch of an individual heavy star is bluer than that of a lighter star. Again, we conclude that the most massive visible stars in M67 are heavier and younger than those in NGC 188.

The preceding arguments have tacitly assumed that composition differences between stars in NGC 188 and M67 are insignificant. Comparing cluster loci with models of composition $(X,Y,Z)=(0.71, 0.27, 0.02)$, one finds that the best fits (16) are obtained for assumed cluster ages of $(5.5\pm1)\times10^9$ yr (for M67) and $(11\pm2)\times10^9$ yr (for NGC 188). With these assignments, the most massive stars in NGC 188 are near $1M_{\odot}$ and no gap in the cluster locus is expected. In fact, the lack of a gap in Sandage's (63) data has been made use of in considerations of goodness of fit.

Sandage (65) has recently re-examined stars in NGC 188 and states that there is evidence for a gap near the turnoff point along the NGC 188 locus. If there is indeed a gap, and no change is made in model initial composition or in the input physics, then the cluster locus for NGC 188 must be raised by at least $\Delta(\log L)\sim0.09$ above the luminosity level assigned by choosing an age of 11×10^9 yr. Upper limits to the ages of M67 and NGC 188 would then be 4×10^9 yr and 8×10^9 yr respectively. On the other hand, the existence of a small convective core is very sensitive to the temperature and density dependences of opacity and of nuclear-burning rates and no special virtue attaches to the composition $(X,Y,Z)=(0.71, 0.27, 0.02)$. The occurrence of a gap in the NGC 188 locus would therefore be far from an embarrassment. On the contrary, it would be an additional constraint which would help narrow the range of acceptable composition variables for stars in NGC 188 and would, it is to be hoped, shed more light on the adequacy of the basic physical assumptions.

THE EVOLUTION OF POPULATION II STARS

Studies of Population II evolution have been hampered by the facts that: (*a*) the helium-to-hydrogen ratio at the surface of most Population II stars is not obtainable spectroscopically; (*b*) the abundance of metals to hydrogen at the surfaces of individual stars may be uncertain by factors of 10; (*c*) there is no *direct* determination of the mass of a single extreme Population II star; (*d*)

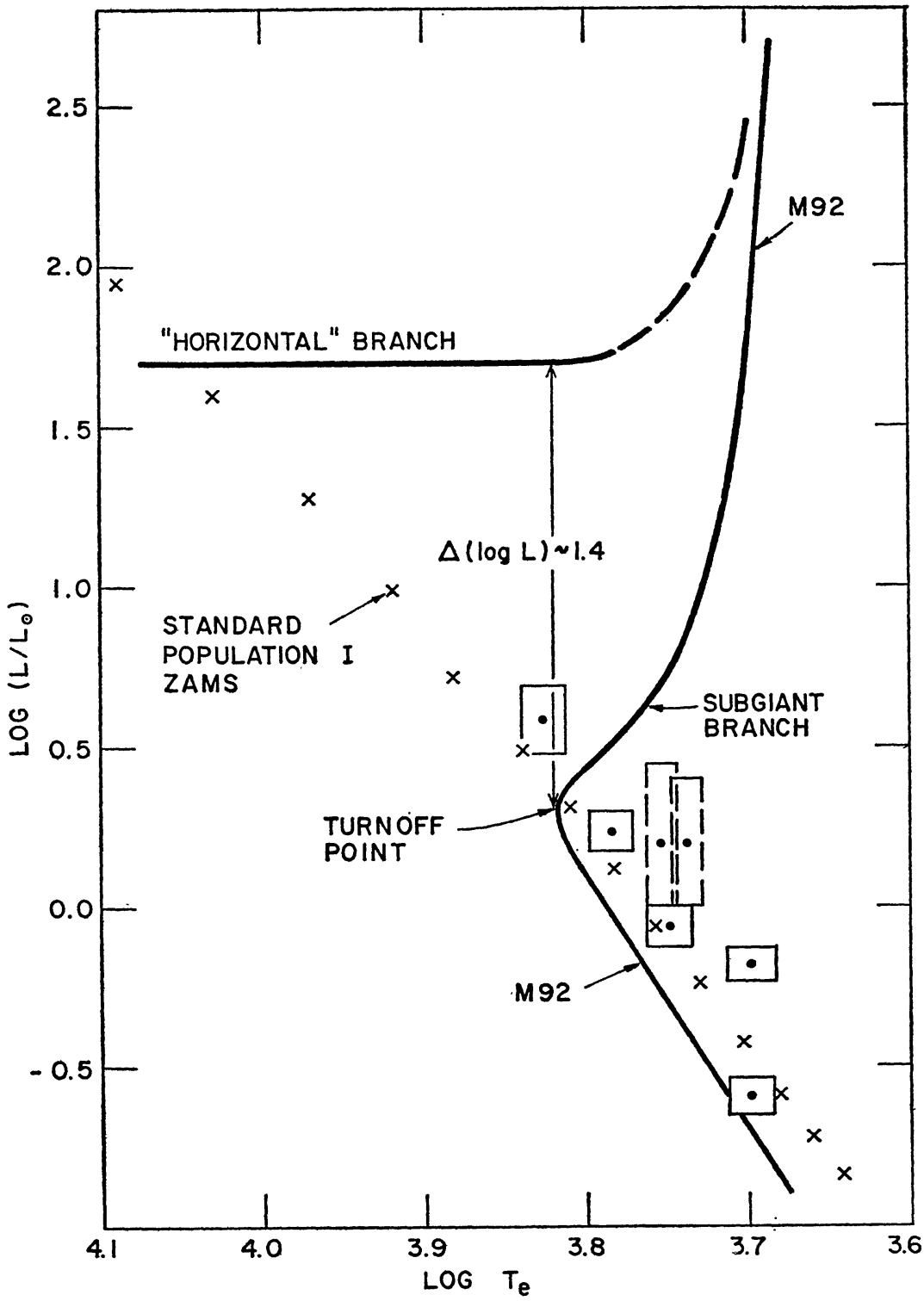

FIG. 12. Observational data for Population II stars. The crosses represent the standard zero-age main sequence for Population I stars. The boxes represent the positions of several subdwarfs as given by Strom, Cohen & Strom (67). The heavy curve is a schematic cluster locus for M92.

the absolute positions of globular cluster stars in the theoretical H-R diagram are highly uncertain; (*e*) the vast majority of Population II stars are in a region of the H-R diagram where the position of theoretical models varies most drastically with changes in the treatment of convective flow in the envelope; (*f*) the calculation of evolution along the giant branch and through the helium-flash phase is very time consuming—a fact which has restricted extensive theoretical exploration.

The type of observational information available for Population II stars is illustrated in Figure 12. Eggen & Sandage (66) have suggested that in the M_{bol}-log T_e plane, metal-deficient subdwarfs form a sequence which coincides, within observational and theoretical errors, with that portion of the zero-age main sequence determined by Hyades stars. The crosses in Figure 12, which define the standard Population I *ZAMS*, may thus represent the location of many Population II stars of low luminosity. Recently S. E. Strom, J. G. Cohen & K. M. Strom (67) have fitted model atmospheres to several subdwarfs for which spectrum scans and trigonometric parallaxes are available. Their results are given by the boxes in Figure 12.

The major features of the cluster locus defined by stars in a typical globular cluster M92 are also sketched in Figure 12. Observational data from Sandage & Walker (68) and from unpublished work by Sandage, as quoted by Sandage & Smith (69), have been used as a guide. The *relative* values of log T_e and log L along the cluster locus for log $L \lesssim 1.7$ are probably correct in order of magnitude. The only fairly reliable *relative* position along the horizontal branch is that of the RR Lyrae stars which lie approximately $\Delta(\log L) \sim 1.4$ above the cluster turnoff point, although the specification of turnoff luminosity is uncertain by perhaps ± 0.1 in log L. That portion of the horizontal branch to the blue of the RR Lyrae region has been drawn arbitrarily at constant luminosity. A fit between the lower portion of the globular-cluster locus and the field subdwarfs can be achieved by moving the sketched locus bodily either horizontally to the red or vertically to higher luminosity (or both). An attempt to specify the absolute position of the cluster locus has been purposely avoided. It is suggested that such an attempt should be made only after spectrum scans have been obtained for a number of cluster stars and model stellar atmospheres have been constructed to fit these scans.

The type of information which may be obtained from model evolution is shown in Figures 13 and 14. In Figure 13, the solid curves are evolutionary paths off the zero-age main sequence for model stars with an initial composition $(X, Y, Z) = (0.9, 0.1, 2\times10^{-4})$, when l/H_{dens} is chosen as 0.5 (70). The dashed curve is the evolutionary path of an $0.75M_\odot$ model which is burning helium in a core of initial mass $0.6M_\odot$ and of initial composition $(X, Y, Z) = (0, 1, 2\times10^{-4})$. The envelope composition of this model is identical with that of the initial main-sequence models. Matter is too cool at the hydrogen-helium interface for hydrogen burning to take place. The dotted curve is merely to indicate that the immediate progenitor of the initial $0.75M_\odot$ model is presumed to be at the red-giant tip.

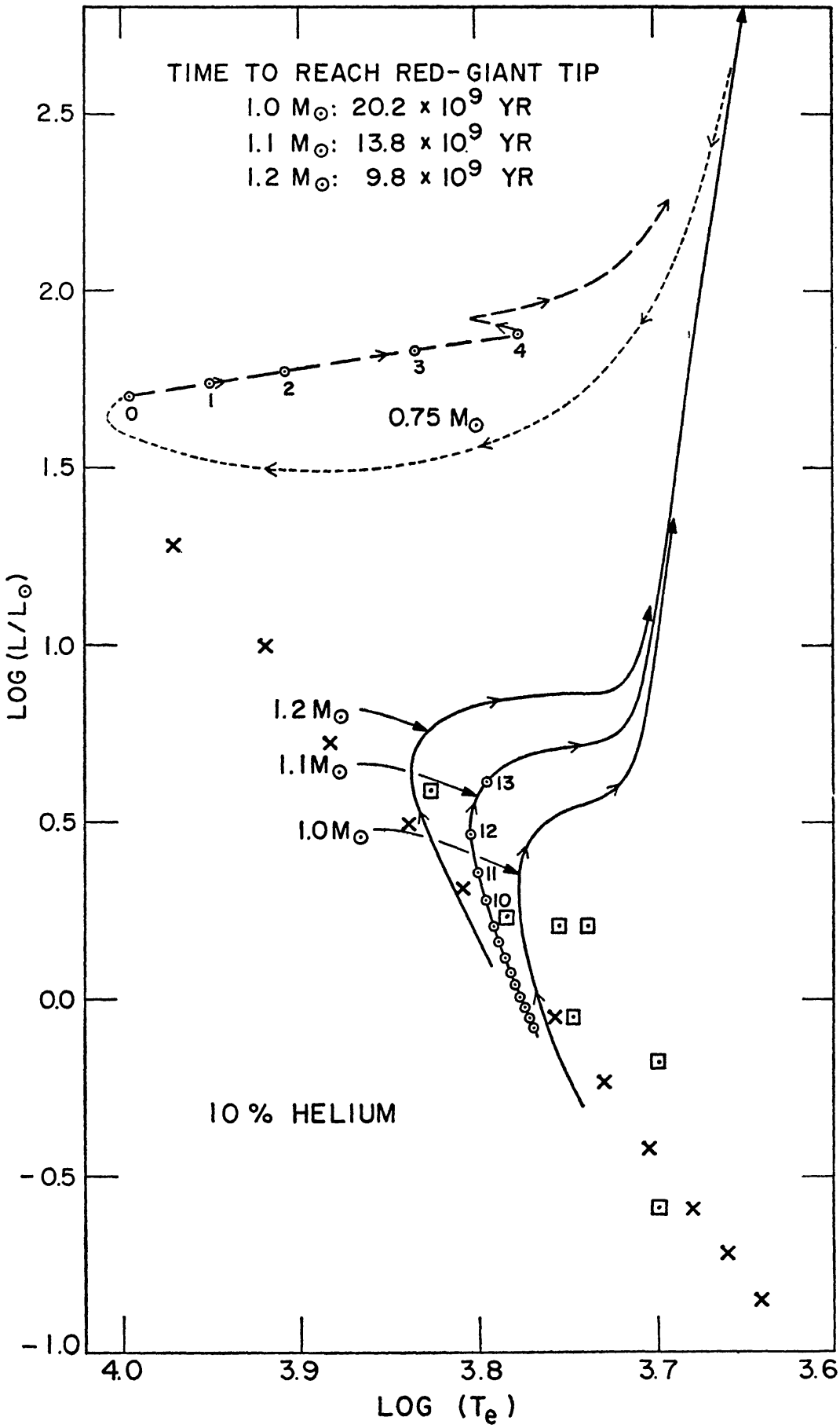

In Figure 14, the solid curves are evolutionary paths for models with an initial composition $(X,Y,Z)=(0.65,\ 0.35,\ 2\times10^{-4})$ and $(l/\mathrm{H_{dens}})=0.5$ (71). The dashed curve (70) is the path of an $0.65M_\odot$ model with a hydrogen-exhausted core of mass $0.4M_\odot$ and an envelope composition identical with that of the initial main-sequence models. Helium is burning in the core but hydrogen burning in the shell provides most of the star's energy output. Again, the dotted curve indicates only an assumed chronological relationship between calculated phases.

The total stellar mass and the mass in the hydrogen-exhausted core of the helium-burning models described in Figures 13 and 14 have been chosen primarily to achieve a mean-luminosity level near $\log L\sim1.7$–1.8 and to achieve the maximum possible extension in $\log T_e$ during the entire phase of core helium burning. The core masses are roughly consistent with the masses in the hydrogen-exhausted core at the start of the helium flash as found by Schwarzschild & Härm (27) and by Hayashi, Hōshi & Sugimoto (3) for the relevant envelope ratios of hydrogen to helium. Further assumptions are that no mixing of hydrogen into the core occurs during the flash (28) and that a negligible amount of helium is burned in the core before degeneracy is lifted.

By a simple extrapolation of the model paths in Figures 13 and 14 to lower masses and luminosities, it is clear that a better fit with the mean of the seven subdwarfs shown can be achieved with the higher choice of initial hydrogen content and an even better fit can be achieved with a choice of 100 per cent initial hydrogen. For each composition, however, an age for several subdwarfs is found to exceed 15–20×10^9 yr.

Demarque (72) has constructed time-constant loci for several choices of initial helium content, the most relevant composition choices for the present discussion being $(X,\ Y,\ Z)=(0.75,\ 0.25,\ 10^{-3})$ and $(0.999,\ 0,\ 10^{-3})$. The mixing-length-to-pressure-scale-height ratio is chosen to be 1. Demarque's time-constant loci are compared with the standard *ZAMS* in Figures 15 and 16. When $X=0.75$, time-constant loci reach the *ZAMS* after 17 billion years; whereas, when $X=0.999$, time-constant loci reach the *ZAMS* in only 11 billion years. Thus, if the standard observational *ZAMS* actually coincides roughly with the lower portion of cluster loci, cluster ages more consistent with that estimated from the Hubble time are achieved with 100 per cent initial hydrogen. On the other hand, ages in excess of 20×10^9 yr are still

---

FIG. 13. Evolutionary paths for metal-poor stars with initial composition $(X,Y,Z)=(0.9,\ 0.1,\ 2\times10^{-4})$. Solid tracks correspond to the phase of pure hydrogen burning. The dashed track describes the evolution of a core helium-burning model with $(M_s,\ M_{\mathrm{core}},\ X_e)=(0.75,\ 0.6,\ 0.90)$. Intervals between consecutive circles along the $1.1M_\odot$ model track correspond to evolutionary times of 10^9 yr. Intervals between circles along the $0.75M_\odot$ track correspond to 10^7 yr. The crosses define the standard *ZAMS* and the boxed points represent positions of field subdwarfs.

necessary to fit several of the extreme subdwarfs in Figure 12 with Demarque's models.

Faulkner & Iben (71) have shown that better agreement in shape with the turnoff region and the subgiant portions of M92 can be achieved with a choice of initial hydrogen content closer to $X=0.65$ than to $X\geq 0.9$. That agreement in shape is better for the lower choice of initial X is evident from comparison between model tracks in Figures 13 and 14 and the cluster locus in Figure 12. This is demonstrated even more convincingly by the corresponding time-constant loci (70). Thus, for *fixed* values of $(l/\mathrm{H_{dens}})\sim 0.5$, better shape fits with some portions of cluster loci can be achieved with a lower value of initial X, whereas better fits with the estimated *absolute* position of extreme subdwarfs and the position of the lower portion of cluster loci, if coincident with the *ZAMS*, can be achieved with a higher value of initial X. This illustrates the danger of accepting conclusions based on attempted fits between model calculations and fragments of the available observational data.

The discussion has thus far proceeded on the assumption that model results are reliable. Unfortunately, during the entire phase of hydrogen burning, the position of every low-mass model of relevance here is highly sensitive to changes in the treatment of convective flow in envelope regions. There is no reason to suppose that a better representation of convective flow might not be achieved by allowing (l/H) to vary with surface temperature, with surface gravity, and with envelope composition. An appropriately chosen time variation of l/H and an improvement in opacities might well result, for any choice of initial $X\geq 0.65$, in adequate fits with extreme subdwarfs and globular-cluster loci and lead to considerably reduced derived ages.

In contrast with the surface temperature, the luminosity of a model star at any given age is unaffected by changes in the treatment of convection. The luminosity at the turnoff point of theoretical time-constant loci is not seriously affected by changes in (l/H). For any choice of composition and input physics, there is a nearly unique relationship between the age, the luminosity at the turnoff, and the mass (assuming no mass loss) of stars along the giant branch. From time-constant loci constructed for the composition and input physics which lead to the model paths in Figures 13 and 14, the entries in Table VI result (70). In this table, t_9 is the assigned age in 10^9 yr,

---

FIG. 14. Evolutionary paths for metal-poor stars with initial composition $(X,Y,Z)=(0.65, 0.35, 2\times 10^{-4})$. Solid tracks correspond to the phase of pure hydrogen burning. The dashed track describes the evolution of a core helium-burning model with $(M_s, M_{\mathrm{core}}, X_e)=(0.65, 0.4, 0.65)$. Intervals between consecutive circles along the $0.7M_\odot$ model track correspond to evolutionary times of 10^9 yr. Intervals between circles along the $0.65M_\odot$ track correspond to 10^7 yr. The crosses define the standard *ZAMS* and the boxed points represent positions of field subdwarfs.

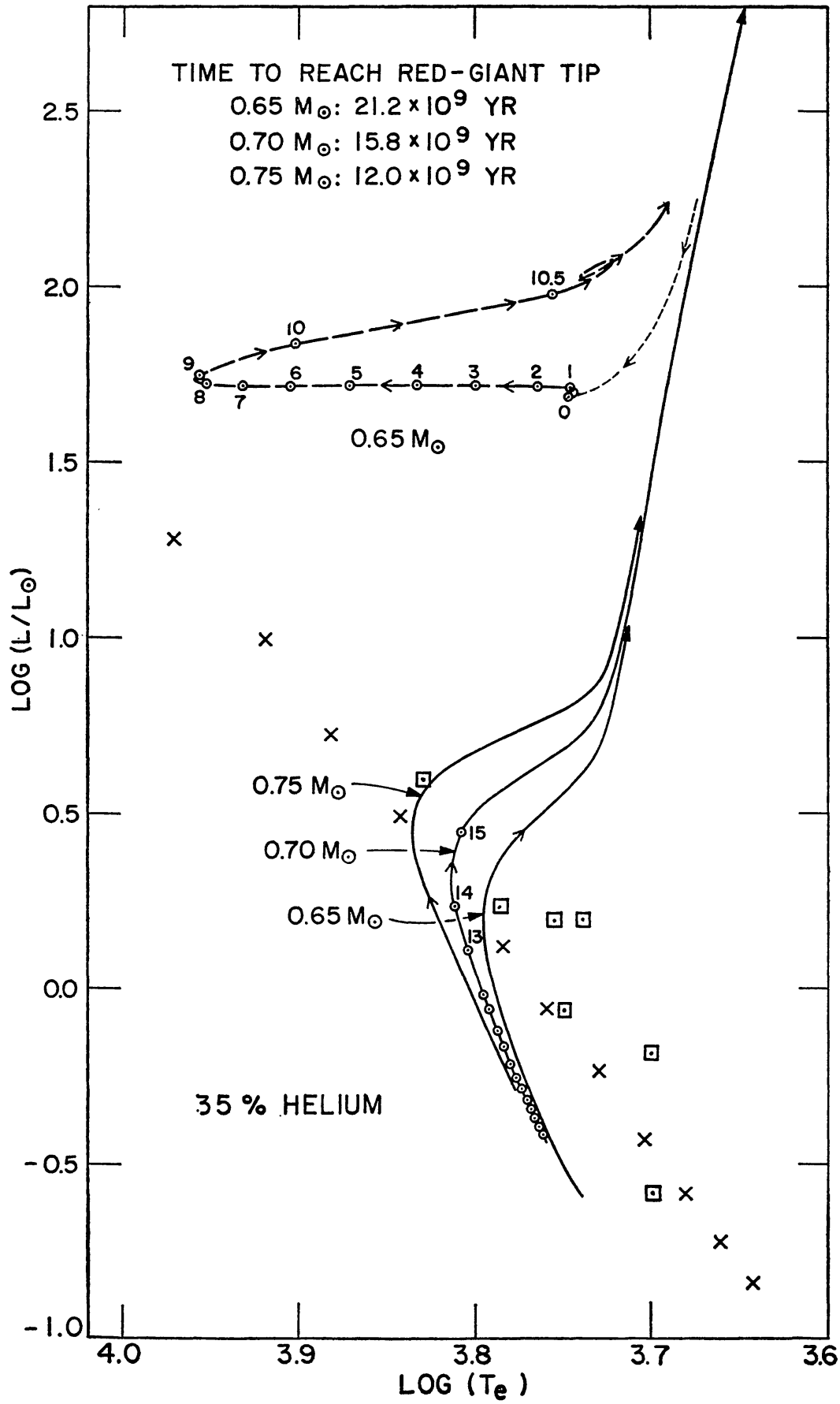

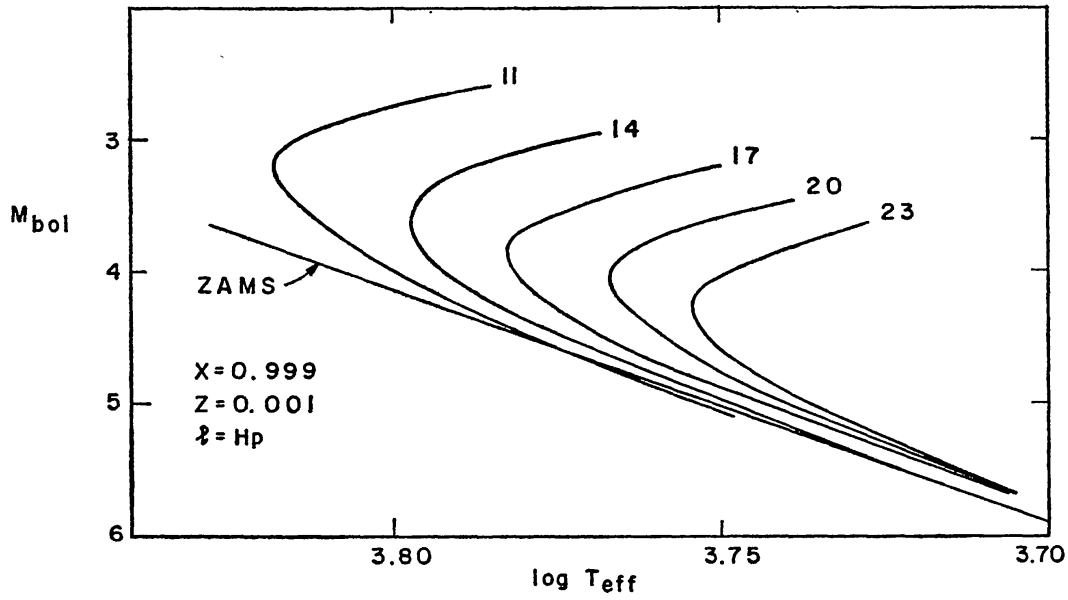

FIG. 15. Time-constant loci obtained by Demarque (72) for the composition $(X,Y,Z)=(0.999, 0, 10^{-3})$.

and L_{to} is the luminosity at turnoff in solar units. The model masses M_{RG} for stars which just reach the red-giant tip in the assigned time are also shown in Table VI. Near $\log L_{to}=0.4$, the relationships between t_9 and L_{to} can be roughly approximated by $t_9 \sim 16.9-39.2\,[\log L_{to}-0.4]$, when $X=0.90$; and $t_9 \sim 13.0-30.8\,[\log L_{to}-0.4]$, when $X=0.65$. Note that for fixed L_{to}, the

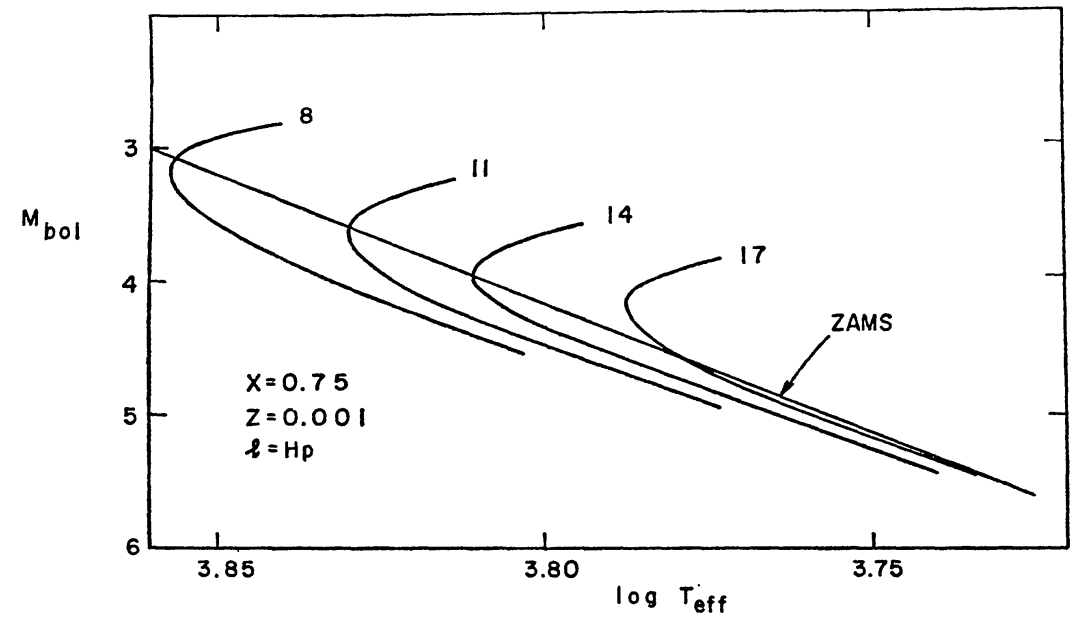

FIG. 16. Time-constant loci obtained by Demarque (72) for the composition $(X,Y,Z)=(0.75, 0.249, 10^{-3})$.

TABLE VI

THE RELATIONSHIP BETWEEN CLUSTER AGE, TURNOFF LUMINOSITY, AND STELLAR MASS ALONG THE GIANT BRANCH

t_9	log (L_{to})		$M/M_\odot$	
	$X=0.65$	$X=0.90$	$X=0.65$	$X=0.90$
8	0.60	0.73	0.82	1.27
10	0.51	0.63	0.78	1.19
12	0.43	0.55	0.75	1.14
14	0.37	0.48	0.72	1.10
16	0.31	0.42	0.70	1.06
18	0.26	0.37	0.68	1.03
20	0.22	0.33	0.66	1.00

cluster age found with $X=0.9$ is 3–4 billion years longer than that found with $X=0.65$.

To illustrate the use of Table VI, suppose that relative surface temperatures along the cluster locus in Figure 12 are correct and that the locus can be moved freely in the vertical direction. If the cluster locus is raised by $\Delta(\log L)\sim 0.3$, the lower portion of the cluster locus lies roughly between the standard *ZAMS* and the mean of the upper six subdwarfs, and the turnoff luminosity occurs at $\log L\sim 0.6$. For $X=0.9$, the cluster age is then $t_9\sim 11$ and the mass of a star along the giant branch is $M_{RG}\sim 1.17M_\odot$. For $X=0.65$, the corresponding numbers are $t_9\sim 8$ and $M_{RG}\sim 0.82M_\odot$. Remember, however, that near the turnoff region and along the subgiant branch, the shape of the cluster locus is not consistent with the theoretical shape for $X=0.9$ and that models with $X=0.65$ do not reach the lower portions of the cluster locus in the allotted time. Remember, too, that surface temperatures along the cluster locus in Figure 12 may well be in error by $\Delta(\log T_e)\sim\pm 0.02$. Shifting the cluster locus in Figure 12 over by $\Delta(\log T_e)\sim -0.02$ and then raising the locus by $\Delta(\log L)\sim 0.15$ would bring the lower portion of the locus into the approximate position achieved by keeping T_e fixed and raising the locus by $\Delta(\log L)\sim 0.3$. The turnoff luminosity would now, however, be at $\log L\sim 0.45$, and values for cluster age and red-giant mass would be $t_9\sim 15$ and $M_{RG}\sim 1.08M_\odot$, for $X=0.90$; and $t_9\sim 11.5$ and $M_{RG}\sim 0.76M_\odot$, for $X=0.65$.

As a result of theoretical studies of RR Lyrae pulsation, Christy (59) has suggested that RR Lyrae variables in very metal-weak clusters are at a luminosity given by $\langle\log L\rangle_{RR}\sim 1.66$. If we allow an error of ± 0.1 in the observational result (68, 69) that RR Lyrae variables in metal-poor clusters lie above the cluster turnoff by $\langle\log L\rangle_{RR}-\log L_{to}\sim 1.4$, then Christy's result places the cluster turnoff at $\log L_{to}\simeq 0.26\pm 0.1$. Extrapolating from Table VI we conclude that, for $X=0.90$, cluster age is $t_9\sim 22.5\pm 4$, whereas for $X=0.65$, cluster age is $t_9\sim 18\pm 4$. Thus, ages long compared to that expected

from the Hubble time are found for both choices of initial X, but smaller ages are found for smaller X. This is exactly the reverse of the conclusion reached by fitting time-constant loci to the *ZAMS*.

The most remarkable result of attempts to fit the horizontal branch with models characterized by an envelope helium content $Y \lesssim 0.1$ is that model mass must be chosen considerably smaller than that appropriate for approximate fits near and beyond the turnoff region. Hayashi et al. (3) were the first to discover this fact, subsequently confirmed by others (71, 73).

For the $0.75 M_\odot$ model shown in Figure 13, the mean luminosity during the phase of core helium burning is roughly $\langle \log L \rangle_{HB} \sim 1.8$. During the last quarter of the phase of core helium burning, where pulsation of the RR Lyrae type might be expected to occur, the mean luminosity is $\langle \log L \rangle_{RR} \sim 1.85$. Let us assume that $\log L_{to} = 1.85 - 1.4 = 0.45$. Then, if we agree that the $0.75\ M_\odot$ model path in Figure 13 provides an adequate fit to the horizontal branch, cluster age is $t_9 \sim 15$, the mass of stars along the giant branch (without mass loss) is $M_{RG} \sim 1.08$, and it is necessary to assume that $\gtrsim 0.33 M_\odot$ has been lost by a star prior to reaching the horizontal branch.

For $X_e = 0.9$, an increase of $\sim 0.05 M_\odot$. in *either* M_s *or* M_{core} leads to increases of about 0.1 in both $\langle \log L \rangle_{HB}$ and $\langle \log L \rangle_{RR}$ (70, 71). If the turnoff luminosity is chosen as $\log L \sim 0.6$, then $\langle \log L \rangle_{RR} \sim 2.0$. A fit to the horizontal branch might then be achieved with a helium-burning model of total mass $M_s \sim 0.8 M_\odot$ and of core mass $M_{core} \sim 0.65 M_\odot$. Since the cluster characteristic M_{RG} is $\sim 1.17 M_\odot$, it must be assumed that a star loses $\sim 0.37 M_\odot$ at some time during the pure hydrogen-burning phases preceding the horizontal-branch phase.

When the envelope abundance of hydrogen is chosen to be $X_e = 0.65$, models burning helium in the core evolve to the blue. For the model characterized by $(M_s,\ M_{core}) = (0.65 M_\odot,\ 0.4 M_\odot)$, both $\langle \log L \rangle_{HB}$ and $\langle \log L \rangle_{RR}$ are about 1.72 (see Figure 14). If the age of globular-cluster stars is chosen to be $t_9 = 15$, then the turnoff luminosity occurs at $\log L_{to} \sim 0.32$ and the horizontal-branch model path in Figure 14 bears the correct relationship to the turnoff luminosity. For $t_9 = 15$, the mass of stars along the giant branch is $\sim 0.7 M_\odot$ and very little mass loss is demanded by fits to the two most distinctive characteristics of cluster loci—the steep subgiant branch and the horizontal branch. This is in strong contrast with the case $X_e = 0.9$ which requires that $0.3 - 0.4 M_\odot$ be lost by a star prior to reaching the horizontal branch.

If the age of globular-cluster stars is chosen to be $t_9 = 10$, and $X_e = 0.65$, then the mass of stars along the cluster giant branch is $M_{RG} \sim 0.78$, the luminosity at the cluster turnoff point is given by $\log L \sim 0.5$ and, therefore, $\langle \log L \rangle_{RR} \sim 1.9$. When $X_e = 0.65$, the value of $\langle \log L \rangle_{HB}$ is less sensitive to changes in M_s and M_{core} than is the case when $X_e = 0.9$. An increase in either M_s or M_{core} by $0.05 M_\odot$ increases $\langle \log L \rangle_{HB}$ and $\langle \log L \rangle_{RR}$ by about 0.06 (70). If, then, $\langle \log L \rangle_{RR} \sim 1.9$, the horizontal branch may be reached by models characterized by $(M_s,\ M_{core},\ X_e) \sim (0.75 M_\odot,\ 0.45 M_\odot,\ 0.65)$ and

essentially no mass loss is required to fit all portions of globular cluster loci.

Comparing the luminosity function for the cluster M13 with model results, Simoda & Kimura (74) have derived semi-empirical estimates for the lifetime of stars along the horizontal branch. For $X_e=0.90$ and an assumed cluster age of 17×10^9 yr, they find $t_{HB}\sim8\times10^7$ yr; for $X_e=0.65$ and an assumed cluster age of 13.5×10^9 yr, $t_{HB}\sim5\times10^7$ yr. Adopting a cluster age of $\sim10^{10}$ yr, these results may be scaled down to $t_{HB}\sim5\times10^7$ yr, for $X_e=0.90$, and $t_{HB}\sim4\times10^7$ yr, for $X_e=0.65$.

For the choice $(M_s, M_{core}, X_e)\sim(0.75, 0.6, 0.9)$ the theoretical horizontal-branch lifetime is $t_{HB}\sim4\times10^7$ yr and $\langle\log L\rangle_{RR}\sim1.85$. An increase in $\langle\log L\rangle_{HB}$ by about 0.15 reduces this lifetime by about 10^7 yr to $t_{HB}\sim3\times10^7$ yr (70). Thus, when $X_e\sim0.9$, a choice of cluster age in the neighborhood of 10^{10} yr or larger leads to theoretical horizontal-branch lifetimes roughly two times smaller than the semi-empirical estimates of t_{HB}.

The theoretical horizontal-branch lifetime for the choice $(M_s, M_{core}, X_e)\sim(0.65, 0.4, 0.65)$ is $t_{HB}\sim10^8$ yr. An increase in $\langle\log L\rangle_{HB}$ by 0.2 leads to a reduction in t_{HB} by a factor of 2 (70). Thus, for $X_e=0.65$, consistency between the model determination and the semi-empirical determination of t_{HB} may be achieved when cluster age is chosen to be $\sim10^{10}$ yr. Agreement becomes more difficult to achieve as the assumed cluster age is increased above 10^{10} yr.

It would be unwise to place too much weight on comparisons with semi-empirically determined values of t_{HB}. These might easily be wrong by factors of 2. In the case of $X_e=0.9$, the semi-empirical determination of t_{HB} may be objected to on the ground that it is based on calculational results for hydrogen-burning models of constant mass, whereas it is necessary to assume significant mass loss at some point during the phase of pure hydrogen burning in order to account for the horizontal-branch stars. If the rate of mass loss is correlated with the violence of subphotospheric turbulence, one might expect mass loss to occur most prominently along the giant branch and lead to giant-branch lifetimes, and hence semi-empirically determined values of t_{HB}, considerably different from those calculated on the assumption of no mass loss.

Christy (59) finds that best fits to pulsational properties of cluster variables occur when model masses are chosen in the neighborhood of $0.5M_\odot$, with a possible spread over the range $0.45M_\odot$ to $0.6M_\odot$. Such low masses are consistent with the values of M_s and M_{core} required to obtain $\langle\log L\rangle_{HB}\sim1.66$ with evolutionary models characterized by an envelope hydrogen abundance $X_e=0.65$. They are not consistent with evolutionary model predictions for $X_e\geq0.9$, which suggest that the mass in the hydrogen-exhausted core is at least $M_{core}\sim0.6M_\odot$ (even larger when plasma neutrino losses are included).

Stars along the blue end of the horizontal branch are hot enough to permit a possibly meaningful determination of the surface ratio of helium to hydrogen. Helium lines in globular-cluster and halo B stars (75–77) are known to

be weak, and a conventional analysis (75) suggests a surface ratio $(Y/X)_e \lesssim 0.03$. Greenstein, Truran & Cameron (78) have argued that gravitationally induced diffusion inward may be responsible for the apparent deficiency in the surface helium abundance. Since elements heavier than helium are affected by diffusion even more strongly than is helium, it should be possible to verify or discard this suggestion by comparing the metal-to-hydrogen ratio in blue horizontal-branch stars with this same ratio in stars along the giant branch of the same cluster. Since convection insures thorough mixing over a large fraction of a giant-branch star's mass, the metal-to-hydrogen ratio in such stars should be much larger than it is in blue horizontal-branch stars—if diffusion is capable of effecting a mass segregation.

In this connection, it is interesting that a value of $(Y/X)_e \sim 0.03$ for matter in the envelope of helium-burning stars is consistent with model predictions when an initial hydrogen abundance of $X = 1$ is assumed. Faulkner & Iben (70) find that as a $1.3 M_\odot$ model with an initial value of $X \simeq 1.0$ evolves up the giant branch, envelope convection extends into the region where considerable helium has been formed during the main-sequence phase. Just before the base of the convective zone begins to recede outward as a consequence of the advancing hydrogen-burning shell, the helium abundance in the envelope reaches the value $Y \simeq 0.03$! If mass loss occurs along the giant branch, then the final surface value of Y may be even larger than this.

It should by now be apparent that a satisfactory interpretation of Population II evolution is not yet within our grasp. An attempt has been made to present as many divergent elements of the puzzle as possible, illustrating that in order to achieve consistency with some shreds of evidence it is necessary to forfeit consistency with other shreds. The strongest support for a very low initial helium content Y comes from the apparent position of extreme subdwarfs in the H-R diagram. The strongest support for an unconventionally high initial Y comes from theoretical studies which indicate that (*a*) pulsation of the RR Lyrae type requires a high envelope Y and a stellar mass small compared to the mass in the helium core of luminous, low-initial-Y red giants and (*b*) globular-cluster shapes are more easily matched and no significant mass loss is required for large values of initial Y. However, regardless of whether high or low Y is correct, a conflict exists between the theory of stellar evolution, the theory of stellar pulsation, and the Hubble time t_H, if, as conventionally supposed, $(2/3)t_H$ is indeed an upper limit to cluster age. Ages near $(2/3)t_H$ could be assigned by evolutionary theory to globular clusters if RR Lyrae stars had luminosities closer to $\langle \log L \rangle_{RR} \sim 1.9-2.0$ than to $\langle \log L \rangle_{RR} \sim 1.6-1.7$, as indicated by pulsation theory. But then the masses of RR Lyrae stars obtained from evolutionary calculations would be significantly larger than the masses suggested by pulsation theory.

LITERATURE CITED

1. Schwarzschild, M., *Stellar Structure and Evolution* (Princeton Univ. Press, Princeton, N. J., 1958)
2. Burbidge, E. M., Burbidge, G. R., *Handbuch der Physik*, **51**, 134 (1958)
3. Hayashi, C., Hōshi, R., Sugimoto, D., *Progr. Theoret. Phys. Suppl. No. 22*, 1 (1962)
4. Sears, R. L., Brownlee, R. R., in *Stellar Structure*, 575 (Aller, L. H., McLaughlin, D. B., Eds., Univ. of Chicago Press, Chicago, Ill., 1965)
5. Langer, E., Herz, M., Cox, J. P., *Joint Inst. Lab. Ap. Rept. No. 88* (Univ. of Colorado, Boulder, Colo., 1966)
6. Kippenhahn, R., *Mitteilungen der Astronomischen Gesellschaft*, 53 (1965)
7. Weigert, A., *Mitteilungen der Astronomischen Gesellschaft*, 61 (1965); *Z. Ap.*, **64**, 395 (1966)
8. Kippenhahn, R., Thomas, H. C., Weigert, A., *Z. Ap.*, **61**, 241 (1965); **64**, 373 (1966)
9. Hofmeister, E., *Z. Ap.*, **65**, 164, 194 (1967)
10. Iben, I., Jr., *Ap. J.*, **140**, 1631 (1964); **143**, 483 (1966)
11. Schönberg, M., Chandrasekhar, S., *Ap. J.*, **96**, 161 (1942)
12. Schwarzschild, M., Härm, R., *Ap. J.*, **142**, 855 (1965)
13. Iben, I., Jr., *Ap J.*, **138**, 452 (1963)
14. Iben, I., Jr., *ibid.*, **142**, 1447 (1965)
15. Iben, I., Jr., *ibid.*, **143**, 505, 516 (1966)
16. Iben, I., Jr., *ibid.*, **147**, 624 (1967)
17. Iben, I., Jr., *ibid.*, 650 (1967)
18. Iben, I., Jr., Ehrman, J. R., *Ap. J.*, **135**, 770 (1962)
19. Pearce, W. P., Bahng, J., *Ap. J.*, **142**, 164 (1965)
20. Stothers, R., *Ap. J.*, **144**, 959 (1966)
21. Schwarzschild, M., Härm, R., *Ap. J.*, **129**, 637 (1959)
22. Schwarzschild, M., Härm, R., *ibid.*, **128**, 348 (1958)
23. Sakashita, S., Ôno, Y., Hayashi, C., *Progr. Theoret. Phys.* (*Kyoto*), **21**, 315 (1959)
24. Sakashita, S., Hayashi, C., *ibid.*, **22**, 830 (1959); **26**, 942 (1961)
25. Stothers, R., *Ap. J.*, **138**, 1074 (1963)
26. Mestel, L., *Monthly Notices Roy. Astron. Soc.*, **112**, 598 (1952)
27. Schwarzschild, M., Härm, R., *Ap. J.*, **136**, 158 (1962); **139**, 594 (1964); **145**, 496 (1966)
28. Saslaw, W. C., Schwarzschild, M., *Ap. J.*, **142**, 1468 (1965)
29. Adams, B., Ruderman, M., Woo, C., *Phys. Rev.*, **129**, 1383 (1963)
30. Inman, C. L., Ruderman, M., *Ap. J.*, **140**, 1025 (1964); **143**, 284 (1966)
31. Chiu, H. Y., *Ap. J.*, **137**, 343 (1963)
32. Sandage, A. R., *Ap. J.*, **125**, 435 (1967); **135**, 349 (1962)
33. Eggen, O. J., *Quart. J. Roy. Astron. Soc.*, **3**, 259 (1962)
34. Bodenheimer, P., *Ap. J.*, **142**, 451 (1965)
35. Hodge, P. W., Wallerstein, G., *Publ. Astron. Soc. Pacific*, **78**, 411 (1966)
36. Faulkner, J., Stefensen, G. (Private communication, 1966)
37. Eggen, O. J., *Ap. J. Suppl. No. 8*, 125 (1963)
38. Eggen, O. J., *Ann. Rev. Astron. Ap.*, **3**, 235 (1965)
39. Roxburgh, I. W., *Monthly Notices Roy. Astron. Soc.*, **128**, 157, 237 (1964)
40. Roxburgh, I. W., Griffith, J. S., Sweet, P. A., *Z. Ap.*, **61**, 203 (1965)
41. Roberts, P. H., *Ap. J.*, **137**, 1129 (1963); **138**, 809 (1963)
42. Collins, G. W., *Ap. J.*, **138**, 1134 (1963); (1965); **146**, 914 (1966)
43. Collins, G. W., Harrington, J. P., *Ap. J.*, **146**, 152 (1966)
44. Kraft, R. P., *Ap. J.*, **142**, 681 (1965)
45. Kraft, R. P., Wrubel, M. H., *Ap. J.*, **142**, 703 (1965)
46. Strittmatter, P. A., Sargent, W. L. W., *Ap. J.*, **145**, 130 (1966)
47. Strittmatter, P. A., *Ap. J.*, **144**, 430 (1966)
48. Sweet, P. A., Roy, A. E., *Monthly Notices Roy. Astron. Soc.*, **113**, 701 (1953)
49. Roxburgh, I. W., Strittmatter, P. A., *Monthly Notices Roy. Astron. Soc.*, **133**, 345 (1966)
50. Weymann, R., *Ann. Rev. Astron. Ap.*, **1**, 97 (1963)
51. Kraft, R. P., *Ap. J.*, **144**, 1008 (1966)
52. Kuhi, L. V., *Ap. J.*, **140**, 1409 (1964)
53. Crampin, J., Hoyle, F., *Monthly Notices Roy. Astron. Soc.*, **120**, 33 (1960)
54. Schmidt-Kaler, Th., *Bonn Veröffentl. No. 70*, 1 (1964)
55. Schild, R. E., *Ap. J.*, **146**, 142 (1966)
56. Hofmeister, E., Kippenhahn, R., Weigert, A., *Z. Ap.*, **60**, 57 (1964)
57. Baker, N., Kippenhahn, R., *Ap. J.*, **142**, 868 (1965)
58. Arp, H. C., *Ap. J.* (In press, 1967)
59. Christy, R. F., *Ann Rev. Astron. Ap.*, **4**, 353 (1966); *Ap. J.*, **144**, 108 (1966)

60. Wildey, R. L., *Ap. J. Suppl. No. 8*, 439 (1963)
61. Iben, I., Jr., Talbot, R., *Ap. J.*, **144**, 968 (1966)
62. Hayashi, C., Cameron, R. C., *Ap. J.*, **136**, 166 (1962); *Astron. J.*, **69**, 140 (1964)
63. Sandage, A. R., *Ap. J.*, **135**, 333 (1962)
64. Johnson, H. L., Sandage, A. R., *Ap. J.*, **121**, 616 (1955)
65. Sandage, A. R. (Private communication, 1966)
66. Eggen, O. J., Sandage, A. R., *Ap. J.*, **136**, 735 (1962)
67. Strom, S. E., Cohen, J. G., Strom, K. M., *Ap. J.*, **147**, 1038 (1967)
68. Sandage, A. R., Walker, M. F., *Ap. J.*, **143**, 313 (1966)
69. Sandage, A. R., Smith, L. L., *Ap. J.*, **144**, 886 (1966)
70. Iben, I,. Jr., Faulkner, J. (In preparation, 1967)
71. Faulkner, J., Iben, I., Jr., *Ap. J.*, **144**, 995 (1966)
72. Demarque, P., *Ap. J.* (In press, 1967)
73. Osaki, Y., *Publ. Astron. Soc. Japan*, **15**, 428 (1963)
74. Simoda, M., Kimura, H., *Ap. J.* (In press, 1967)
75. Greenstein, J. L., Munch, G., *Ap. J.*, **146**, 618 (1966)
76. Searle, L., Rodgers, A. W., *Ap. J.*, **143**, 809 (1966)
77. Sargent, W. L. W., Searle, L., *Ap. J.*, **145**, 652 (1966)
78. Greenstein, G. S., Truran, J. W., Cameron, A. G. W., *Nature*, **213**, 871 (1967)